

35

Quantification of the Distribution of Macromolecules in Vascular Tissue

by

Wade K. Wan

B.S., Biomedical Engineering,
Johns Hopkins University, 1995

SUBMITTED TO THE DEPARTMENT OF ELECTRICAL ENGINEERING AND
COMPUTER SCIENCE IN PARTIAL FULFILLMENT OF THE REQUIREMENTS
FOR THE DEGREE OF

MASTER OF SCIENCE IN ELECTRICAL ENGINEERING
AND COMPUTER SCIENCE
AT THE
MASSACHUSETTS INSTITUTE OF TECHNOLOGY

FEBRUARY 1998

© 1998 Wade K. Wan. All rights reserved

The author hereby grants to MIT permission to reproduce and to distribute publicly
paper and electronic copies of this thesis document in whole or in part.

Signature of Author: _____
Department of Electrical Engineering and Computer Science
February 1, 1998

Certified by: _____
Elazer R. Edelman
Thomas D. and Virginia W. Cabot Associate Professor
Division of Health Sciences and Technology
Thesis Supervisor

Accepted by: _____
Arthur C. Smith
Professor of Electrical Engineering and Computer Science
Chair, Committee on Graduate Students

MAR 27 1998

LIBRARIES



Quantification of the Distribution of Macromolecules in Vascular Tissue

by
Wade K. Wan

Submitted to the Department of Electrical Engineering and Computer Science
on February 1, 1998 in Partial Fulfillment of the Requirements for the Degree of
Master of Science in Electrical Engineering and Computer Science

ABSTRACT

Quantitative tools to assess vascular macromolecular distributions have so far been limited by post-experiment artifact, low signal-to-noise ratios, limited spatial resolution, and the inability to provide multi-dimensional drug distribution profiles. This suggests the need to develop new techniques that overcome these limitations. A new technique combining fluorescence microscopy with digital post-processing has been developed. Quantitative fluorescence microscopy studies have been limited by autofluorescence, the process where endogenous compounds emit energy at the same wavelength as fluorescent labels, and the proper conversion of fluorescent intensities to physical concentrations. Specimens were imaged with two different filter sets with one image consisting of signal from both autofluorescent molecules and fluorescent labels and the other image containing signal only from autofluorescence. The latter image is then used to estimate the autofluorescence in the former. Subtraction of the estimated autofluorescence results in an autofluorescence-free image. A standard curve to convert fluorescent intensities to macromolecular concentrations was constructed by examining tissue specimens that were incubated until equilibrium in different concentrations. The end result is a two-dimensional concentration profile with spatial resolution superior to many of the previous methods to quantify macromolecular distributions. To illustrate the utility of this technique, the transvascular transport of fluorescently labeled 20 kD dextrans in the calf carotid artery is examined using an *in vitro* perfusion apparatus. A mathematical model of transport is evaluated using measured concentration profiles yielding estimates of important transport parameters such as the effective diffusivity, and endovascular and perivascular permeabilities. Future experiments incorporating this new technique will be able to elucidate details of macromolecular transport which can then be used to improve the efficacy and efficiency of drug delivery systems.

Thesis Supervisor: Elazer R. Edelman

Title: Thomas D. and Virginia W. Cabot Associate Professor, Division of Health Sciences
and Technology

Acknowledgments

I would first like to thank my thesis supervisor Professor Elazer Edelman for taking me under his supervision and allowing me to join his laboratory. He is a wonderful mentor and has always put aside everything from his incredibly busy schedule to deal with my scientific, academic, and personal matters. He has contributed to both my professional and personal development and provided me with much support and advice. I will never forget his attention to the happiness and needs of the laboratory, passion and dedication for research, and his ability to balance his incredibly demanding schedule. I consider him a role model both as a scientist and a person.

I would like to begin by thanking everyone in the group for all of their time and energy spent helping and teaching me. Interacting with the members of Elazer's laboratory has been rewarding both scientifically and personally. I am extremely grateful to Dr. Mark Lovich for functioning essentially as a co-advisor. He was always eager to see how my work was progressing, constantly suggesting new ideas, and proofread many of my manuscripts. His contributions throughout this work were invaluable. I thank Dr. David Ettenson for answering my numerous questions on topics ranging from biology to computers to the art of writing and having the patience to listen to me work out other problems. I was fortunate to have Jim Squire as my officemate, who was always willing to help my writing by finding the right words to describe my thoughts, work out engineering and programming problems, or provide encouragement. I thank Dr. Tony English for being the comic material that I would use to entertain the whole lab with. More seriously, I thank Tony for always pressuring me to finish writing and am waiting for the day I can congratulate him for all his hard work and perseverance and call him Professor English. I owe thanks to Philip Seifert for teaching me everything that I know about immunohistochemistry, a.k.a. histology, and keeping me entertained during my hours slaving away at the cryostat. I thank Dr. Edward Koo for teaching me the

fundamentals of microscopy. I thank Anna Browne, who took care of so many things to make life easier for me and always did it with a warm smile. Kristy Hong assisted with this research when it was still in its developmental stage and I am sure she is on her way to a successful research career. Thanks to Chao-Wei Hwang, who helped me a great deal with finishing this research and I look forward to assisting him with future extensions of this work. A special thanks to Dr. Chun Yu for all of her support and encouragement.

I would like to thank my academic advisor, Dr. Roger Mark, for all his advice on academic and career decisions. I would also like to thank the Whitaker Foundation for providing me with a graduate fellowship that provided me the freedom to explore laboratories during my first semester and then concentrate on classwork and research without having to worry about financial support. I owe thanks to my two roommates during this time, Chuck Cheung and Rama Mukkamala, who I now join in pursuit of that elusive Ph.D. Thanks to Dr. Aileen Huang, who prepared me for graduate school even before I was a graduate student. I also thank my research advisors back at Johns Hopkins, Dr. Eric Young and Dr. Norman Sheppard, who introduced me to research and helped me get where I am today.

Finally, I would like to thank my parents, Wing-Yuk and Manwai, and brother Jimmy for all their love and support.

Wade Wan

Cambridge, MA

February 1, 1998

Table of Contents

ACKNOWLEDGMENTS.....	3
TABLE OF CONTENTS.....	5
LIST OF FIGURES	7
LIST OF TABLES.....	8
I. INTRODUCTION.....	9
I.A. STATEMENT OF THE PROBLEM	9
I.B. THESIS ORGANIZATION	9
II. BACKGROUND.....	11
II.A. MOTIVATION.....	11
II.B. PROLIFERATIVE VASCULAR DISEASES.....	12
II.B.1. <i>Structure of the Artery</i>	13
II.B.2. <i>Disease States</i>	15
II.B.3. <i>Treatment Options</i>	16
II.C. ASSESSING MACROMOLECULAR DISTRIBUTIONS.....	17
II.C.1. <i>Radioactive Techniques</i>	17
II.C.2. <i>Nonradioactive Techniques</i>	19
II.D. ISSUES WITH QUANTITATIVE FLUORESCENCE MICROSCOPY	21
II.D.1. <i>Autofluorescence</i>	21
II.D.2. <i>Conversion of Intensities to Concentrations</i>	23
II.E. CHAPTER SUMMARY	23
III. QUANTIFICATION OF MACROMOLECULAR DISTRIBUTIONS IN VASCULAR TISSUE.....	25
III.A. INTRODUCTION.....	25
III.B. MATERIALS AND METHODS.....	26
III.B.1. <i>Calibration Standards</i>	26
III.B.2. <i>Immobilization and Sectioning</i>	27
III.B.3. <i>Image Acquisition System</i>	27
III.B.4. <i>Initial Processing</i>	28
III.B.5. <i>Autofluorescence Compensation</i>	28
III.B.6. <i>Conversion of Fluorescent Intensities to Tissue Concentrations</i>	30
III.B.7. <i>Equilibrium Time for Standards</i>	31
III.B.8. <i>Demonstration</i>	32
III.C. RESULTS	33
III.C.1. <i>Autofluorescence Compensation</i>	33
III.C.2. <i>Conversion of Fluorescent Intensities to Tissue Concentrations</i>	35
III.C.3. <i>Demonstration</i>	37
III.D. DISCUSSION	38
III.D.1. <i>Comparison with Other Techniques</i>	38
III.D.2. <i>Autofluorescence Compensation</i>	39
III.D.3. <i>Conversion of Fluorescent Intensities to Tissue Concentrations</i>	41
III.D.4. <i>Future Applications</i>	41

III.E. CHAPTER SUMMARY	42
IV. MEASUREMENT OF TRANSVASCULAR TRANSPORT PARAMETERS.....	43
IV.A. INTRODUCTION	43
IV.B. MATHEMATICAL MODELING.....	44
IV.C. PERFUSION EXPERIMENTS.....	46
IV.D. EXTRACTION OF CONCENTRATION PROFILES FROM IMAGES.....	48
IV.E. DETERMINATION OF TRANSPORT PARAMETERS	49
IV.F. CHAPTER SUMMARY.....	54
V. CONCLUSIONS	55
V.A. ACCOMPLISHMENTS.....	55
V.B. FUTURE DIRECTIONS	55
VI. APPENDIX	57
VI.A. CALCULATING TISSUE CONCENTRATIONS FROM BULK INCUBATION CONCENTRATIONS.....	57
VI.B. DERIVATION OF EQUATIONS FOR A MATHEMATICAL MODEL OF TRANSVASCULAR TRANSPORT	58
VI.C. PROGRAMMING CODE FOR TRANSPORT MODEL AND PARAMETER FITTING ROUTINE.....	60
<i>VI.C.1. Parameter Fitting Routine (ww_trans_fit.m)</i>	60
<i>VI.C.2. Mathematical Model of Transport (ww_trans_model.m)</i>	61
<i>VI.C.3. Error Function (ww_trans_error.m)</i>	63
VI.D. EXPERIMENTAL DATA	64
REFERENCES	67

List of Figures

FIGURE 1. IMAGE OF A CROSS-SECTION OF A CALF CAROTID ARTERY	15
FIGURE 2. POST PROCESSING ALGORITHM TO COMPUTE CONCENTRATION PROFILES	29
FIGURE 3. TISSUE CONCENTRATION AS A FUNCTION OF INCUBATION TIME.....	32
FIGURE 4. SCHEMATIC DIAGRAM OF <i>IN VITRO</i> PERFUSION APPARATUS.....	33
FIGURE 5. CORRELATION BETWEEN UV AND FITC AUTOFLUORESCENCE	34
FIGURE 6. FLUORESCENT INTENSITY AS A FUNCTION OF INCUBATION CONCENTRATION	35
FIGURE 7. TISSUE CONCENTRATION AS A FUNCTION OF BULK PHASE CONCENTRATION	36
FIGURE 8. TRANSVASCULAR CONCENTRATION PROFILES	37
FIGURE 9. CONCENTRATION PROFILES FOR ONE HOUR PERFUSION DATA.....	52
FIGURE 10. CONCENTRATION PROFILES FOR TWO HOUR PERFUSION DATA.....	53

List of Tables

TABLE 1. PARAMETER VALUES AND MEAN-SQUARE ERRORS OBTAINED WHEN FITTING ONE HOUR PERFUSION DATA.....	52
TABLE 2. PARAMETER VALUES AND MEAN-SQUARE ERRORS OBTAINED WHEN FITTING TWO HOUR PERFUSION DATA.....	53
TABLE 3. EXPERIMENTAL DATA FOR FIGURE 3 (TISSUE CONCENTRATION AS A FUNCTION OF INCUBATION TIME).....	64
TABLE 4. EXPERIMENTAL DATA FOR FIGURE 6 (FLUORESCENT INTENSITY AS A FUNCTION OF INCUBATION CONCENTRATION).....	65
TABLE 5. EXPERIMENTAL DATA FOR FIGURE 7 (TISSUE CONCENTRATION AS A FUNCTION OF BULK PHASE CONCENTRATION).....	66

I. Introduction

I.A. Statement of the Problem

Tissue culture and animal studies have elucidated many details about the pathobiology of different diseases and this mechanistic information has suggested a number of biologic and synthetic therapeutic agents. Surprisingly, the tremendous potential of these drugs has not always been realized. Two alternatives arise in describing this paradox; either the drugs are ineffective for their intended use, or they do not reach their intended target at sufficient doses or with necessary timing to elicit the expected response. The issue as to which explanation predominates can be determined by in depth tracking of drug deposition and metabolism. Traditionally known as pharmacokinetics, this field of study has been hindered by limitations in the techniques used to assess the distribution of therapeutic compounds. Such problems are especially prominent in the blood vessel with post-experiment artifact, low signal-to-noise ratios, limited spatial resolution and the inability to acquire multi-dimensional drug distribution profiles. This suggests the need to develop new techniques to quantify concentration profiles to obtain better experimental data.

I.B. Thesis Organization

This thesis describes the development of a new technique to quantitatively assess the distribution of macromolecules in vascular tissue. Chapter 2 introduces the clinical and scientific motivation for developing a new method to measure macromolecular concentration profiles. Chapter 3 discusses the development of this new technique which integrates quantitative fluorescence microscopy with digital post processing. Chapter 4 demonstrates the utility of this new method to measure macromolecular distributions. The new technique is combined with *in vitro* experiments and mathematical modeling to investigate the transvascular transport of fluorescently labeled 20 kD dextrans in the calf

carotid artery. Chapter 5 summarizes the work in this thesis and suggests applications of this work to further understanding of the pharmacokinetics following drug delivery.

II. Background

II.A. Motivation

Modern medicine has identified the molecular and biochemical defects of many diseases. For example, proliferative vascular diseases have been shown to result from a disruption of the normal checks and balances and sophisticated nature of cell-cell and cell-tissue relationships (Ross 1993). Delineation of specific endogenous compounds that inhibit and/or promote homeostasis have suggested avenues for the administration of vasotherapeutic compounds to specific portions of the blood vessel wall. As in general pharmacology, therapeutic options for vascular disease include an increasing number of potential biologic and synthesized agents. Yet the administration of these drugs is not straightforward, and is complicated by narrow therapeutic ranges, and short half-lives. When there exists minor differences between drug levels that are subtherapeutic, efficacious, and toxic, for agents that may also be quickly degraded or cleared by the circulatory system before they exert their biologic effect, problems arise.

The sustained release of such drugs might help regulate drug concentrations within defined therapeutic ranges for prolonged periods of time. These ideas can be obtained by a variety of delivery devices, including those that involve pumps or polymeric devices (Langer and Moses 1991; Nimni 1997). Many studies have quantified drug release for different delivery strategies. However, further research is required as the release characteristics of these delivery systems only partially determines the efficacy of the delivered compound. In addition to the pattern of drug release, the biologic effect of an administered compound is determined by its *transport*, *deposition*, and *clearance*. *Transport* refers to the propagation of the agent through tissue, *deposition* is the localization of the bioactive compound, and *clearance* determines the duration that the compound can exert its biologic effect. Like release, the quantitative detection of each of

these three phenomena is determined by the sensitivity and resolution of the techniques available.

To date, quantitative tools to assess vascular distribution of macromolecules have so far been limited by post-experiment artifact, low signal-to-noise ratios, spatial resolution, and the inability to provide multi-dimensional drug distribution profiles. These issues have restricted experiments on the pharmacokinetics after administration, suggesting that new techniques be developed. Once available, sensitive techniques could be utilized to gain insight into pharmacological delivery strategies and devices. It would be especially helpful, for example, to know if a pharmacological failure arises from biological inefficacy or from inadequate distribution. In addition to improving the efficiency and successfulness of pharmacological therapy, this research will elucidate details of blood vessel physiology and homeostasis in states of health and disease.

II.B. Proliferative Vascular Diseases

Many areas of medical research could utilize techniques to assess drug concentrations in tissue to further understanding of the underlying physiology and assist the design of potential pharmacological therapies. One field where these techniques could have substantial impact is the treatment of proliferative vascular diseases. These diseases are the leading cause of morbidity and mortality in the world today, accounting for over 1 million deaths and almost 1.5 million interventions each year in the United States alone. Tissue culture and animal studies have elucidated many of the details concerning pathobiology of these diseases, but all treatments developed so far have only had temporarily benefits. Mechanical revascularizations such as percutaneous transluminal coronary angioplasty and endovascular stent placement have inevitably been followed by accelerated vascular diseases in response to the mechanical injury (Schwartz, Huber et al. 1992; Rogers and Edelman 1995). Many pharmacological agents have also been developed to treat proliferative vascular diseases either alone or in conjunction with mechanical revascularization. However, the tremendous potential of pharmacological

therapies has been limited by the lack of understanding of the pharmacokinetics within the vessel wall. This is partly the result of limitations in current techniques to measure the vascular distribution of compounds such as low spatial resolution. The development of tools to assess vascular distributions and insight gained from experiments using these techniques is needed to realize the potential of proposed pharmacological therapies. A review of vascular architecture and physiology will put into context many of the terms and concepts used in this work.

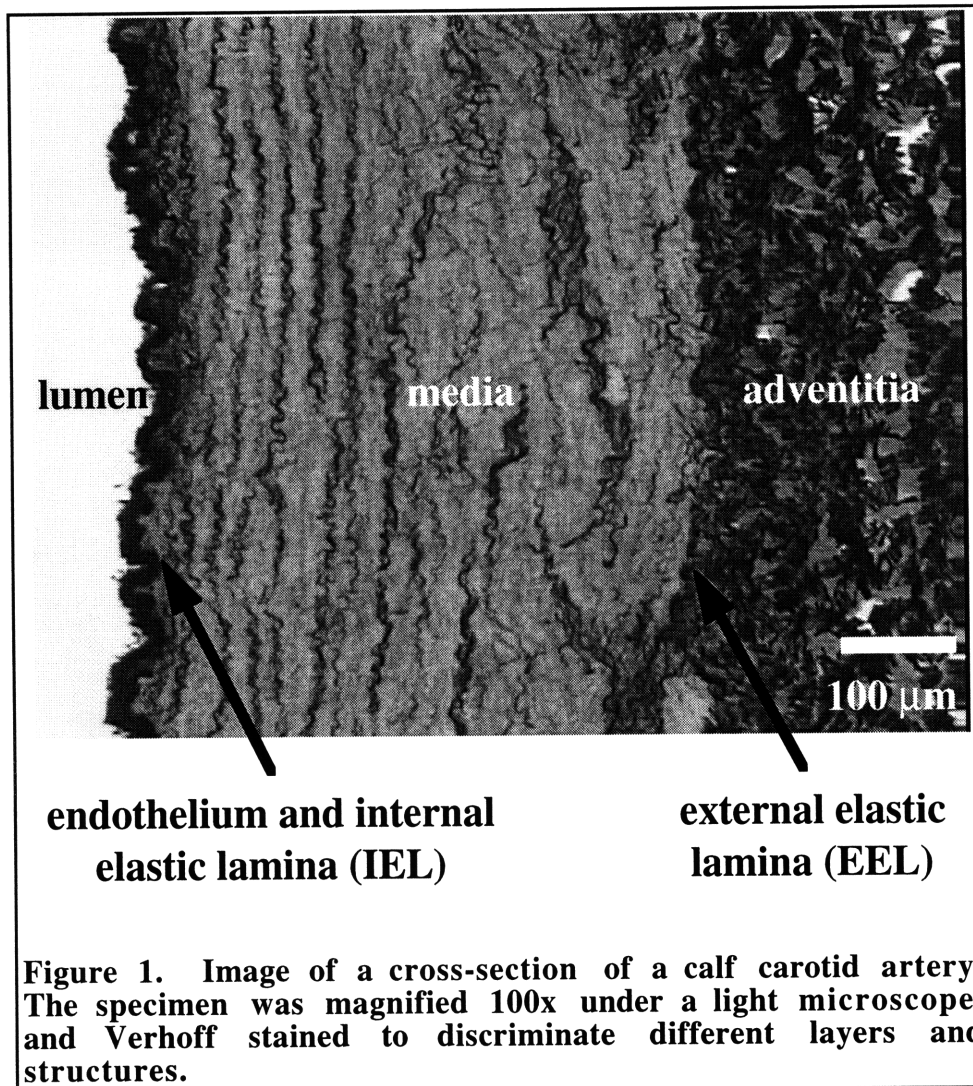
II.B.1. Structure of the Artery

Arteries are best described as vascular structures that carry blood away from the heart to distal tissues. They are comprised of three morphologically distinct concentric tunics or layers. The innermost layer, the *tunica intima*, is composed of a monolayer of endothelial cells supported by the internal elastic lamina, a layer of connective tissue comprised mainly of elastin. In addition to being thromboresistant and transducing signals for cells within the arterial wall, the endothelium modulates transport for many compounds between the vessel wall and the interior of the artery known as the lumen or endovascular space. In humans and higher animal species, there may also be some vascular smooth muscle cells between the endothelial monolayer and the internal elastic lamina. The middle layer, the *tunica media*, is composed of circumferentially aligned smooth muscle cells and thin sheets of connective tissue such as collagen and elastin. The contraction and relaxation of smooth muscle cells modulates the vessel diameter, controlling the perfusion through the artery to downstream tissues. The media is separated from the outermost layer, the *tunica adventitia*, by a fenestrated sheet of elastin, the external elastic lamina. The adventitia is composed primarily of type I collagen with loosely arranged fibroblasts and smooth muscle cells. The adventitia gradually blends into the surrounding fascia and fat, sometimes referred to as the perivascular space. In arteries that are approximately 0.5 mm or thicker, this layer

contains *vasa vasorum*, blood vessels within the blood vessel wall, that help perfuse cells within the vessel wall.

Cells in the arterial wall can communicate with, and regulate each other, by secreting biochemical compounds. For example, the release of growth factors such as endothelial-derived relaxation factor (EDRF) or nitrous oxide (NO) by endothelial cells causes smooth muscle cells in the media to relax, resulting in vasodilation and increased blood flow to downstream tissues. Biochemical signals can also promote and inhibit the growth of other cells, thereby controlling vascular structure and function. Injured vascular smooth muscle cells secrete compounds such as basic fibroblast growth factor (bFGF) which are mitogenic to both endothelial and smooth muscle cells. This process appears to be a part of the natural reparative response of the vessel wall. Confluent endothelial cells secrete compounds such as heparan sulfate proteoglycans (HSPG) which inhibit smooth muscle cell growth that may provide negative feedback to healing processes. Vascular function is dependent on cells communicating and regulating each other, and dysfunction of these processes often leads to disease states.

In the calf carotid artery, the animal model that will be used in studies described later in this work, the diameter of the artery is 3-4 mm and the thicknesses of the intima, media, and adventitia are approximately 100-200 μm , 300-400 μm , and 200-300 μm , respectively. Figure 1 shows a cross-section of a calf carotid artery magnified 100x under a light microscope. The specimen in Figure 1 has been Verhoff stained to highlight elastin, a common component of the vessel wall. This figure illustrates the inhomogeneity of vascular tissue which complicates modeling of transport within the vessel wall.



II.B.2. Disease States

The most prevalent cardiovascular disease is atherosclerosis, the formation of thickened and hardened lesions in medium and large muscular and elastic arteries. The atherosclerotic process probably begins as a reparative response to injury and/or dysfunction of the endothelium and/or smooth muscle cells. Leukocytes and macrophages adhere to the vessel and migrate subendothelially. The macrophages accumulate lipids, forming fatty streaks in the vessel wall. Some of the macrophages may emigrate back into the bloodstream after pushing apart thromboresistant endothelial cells, resulting in thrombosis at the injured site and the release of potent growth promoting

factors in response to this vascular injury. Various forms of the hyperproliferative response cause the progression of the fatty streak to fibrofatty and fibrous lesions in the intima. These lesions cause the vessel to lose its elasticity and narrow the lumen, limiting the blood supply to downstream tissues and/or organs.

II.B.3. Treatment Options

Treatment of proliferative vascular diseases has not been straightforward. Currently, mechanical interventions, such as endovascular stenting, balloon angioplasty, and bypass surgery, are the default therapies. The temporary increase in vessel diameter has inevitably been followed by renarrowing of the lumen due to the reparative response to the mechanical injury, referred to as intimal hyperplasia or restenosis. Pharmacological therapies are also being investigated, but despite cell culture and animal studies which have suggested classes of bioactive compounds that should limit these diseases, none have been successful clinically. Pharmacological therapy can be classified into two categories: systemic and local delivery. Systemic administration such as by intravenous injection requires the agent to circulate throughout the body. Systemic delivery is often ineffective because the non-specificity of many compounds can injure nontarget tissues and organs, the marked systemic toxicity of some compounds, and rapid degradation of others. Local administration attempts to deliver drugs to a specific site, and can be classified by the pattern of delivery. Bolus delivery can be obtained from permeable balloon catheters and sustained delivery from devices such as polymeric release formulations which can be implanted on or near the endovascular and perivascular surfaces. The potential to deliver therapeutic levels of drugs without adverse systemic effects has made local delivery an exciting area of research. This new technology has only recently begun to be studied rigorously and may be more difficult to analyze than systemic delivery because of the small quantities of drug being used. The use of local concentration gradients suggests that it is very important to understand the transport and deposition of compounds following administration.

II.C. Assessing Macromolecular Distributions

Both radioactive and nonradioactive techniques have been developed to quantitatively assess macromolecular distributions. A review of developed techniques will demonstrate the limitations of current methods and the necessity to develop a new technique that overcomes some of these limitations.

II.C.1. Radioactive Techniques

Most pharmacokinetic studies have tracked the compound of interest by labeling it with radioactive nuclides, such as tritium (^3H) or radioiodine (^{125}I). Detection and measurement of radioactivity is usually straightforward and attachment of a radiolabel minimally changes the physical structure of a compound and its transport properties. Radioactivity counts can then be converted to physical concentrations of the compound of interest. However, studies utilizing radiolabels often have limited spatial resolution and are complicated by environmental and health hazards.

A simple, low spatial resolution method to quantify deposition is to count the radioactivity in bulk tissue sections (Duncan, Buck et al. 1963). This method is commonly used in studies with small tissues that are difficult to reliably section with a microtome. Yet, it is limited by its spatial resolution and repeatability, and only measures the average radioactivity for a bulk tissue section without providing a quantitative description of the distribution within the tissue. In addition to assessment of net drug within bulk tissue sections, radioactive counts of the endovascular and perivascular solutions can be integrated with a mathematical model to analytically solve for transport parameters. Previous work in our laboratory has demonstrated the utility of this approach for examining the transmural transport of tritium-labeled heparin in the rat abdominal aorta (Lovich and Edelman 1995).

Higher spatial resolution can be obtained for tissues large enough to be sectioned with a microtome. The artery can be sliced longitudinally, unfolded, and sectioned

parallel to the intimal surface. The radioactivity of these *en face* serial sections can be used to construct one-dimensional transvascular concentration profile. This technique is commonly used to study the transport of a variety of compounds in different animal models including the movement of radioiodinated albumin in the abdominal aorta of the rat (Tedgui, Merval et al. 1992) and young pig (Bell, Adamson et al. 1974), and rabbit thoracic aorta (Bratzler, Chisolm et al. 1977; Ramirez, Colton et al. 1984), radioiodinated fibrinogen in the normal pig abdominal aorta (Bell, Gallus et al. 1974), and radioiodinated low-density lipoprotein in the rabbit thoracic aorta (Bratzler, Chisolm et al. 1977). The resolution of this technique is limited by the fact that slice thicknesses of 10-20 μm are required for reliable sectioning. Axial or circumferential concentration profiles may be obtained by orientating the artery differently in the microtome, but this technique cannot be adapted to provide multi-dimensional distribution profiles of a single specimen.

Another method for converting the signal from radiolabels to macromolecular concentrations is autoradiography or microautoradiography (Aitken, Wright et al. 1968; Fry, Mahley et al. 1980; Schnitzer, Morrel et al. 1987; Tompkins, Yarmush et al. 1989). This involves sectioning the tissue in cross-section, juxtaposing these sections to specially prepared photographic film, and exposing the film for days to months. A linear relationship between the silver in the developing film and its exposure to radiation allows intensities of grains in the film to be converted to concentrations, creating a two-dimensional concentration profile. There are many different variations of this commonly used technique. Microautoradiography differs from autoradiography in that the section is dipped into an emulsion silver preparation which then acts as the developing media. Dipping the specimen into the silver preparation reduces the scatter from each radioactive source since the source and developing media are closer together, but may cause soluble compounds to diffuse resulting in loss of signal and artifact. This resolution of these techniques (1 or 2 μm) is limited by inaccurate localization due to scatter from each radioactive source and the grain size of the photographic film. The duration needed to expose the photographic film may be inconvenient for certain studies. Tissue sections

have been exposed for up to 308 days to accurately measure low concentrations of radioiodinated proteins (Schnitzer, Morrel et al. 1987).

II.C.2. Nonradioactive Techniques

Nonradioactive markers such as Evans-blue (Chuang, Cheng et al. 1990), horseradish peroxidase (Penn, Koelle et al. 1990) and various fluorescent tags, such as fluorescein isothiocyanate (FITC) (Nakamura and Wayland 1975; Fox and Wayland 1979; Nugent and Jain 1984; Castellot, Wong et al. 1985; Armenante, Kim et al. 1991), 1,1'-dioctadecyl 3,3,3',3' tetramethylindocarbocyanine (DiI) (Rutledge, Curry et al. 1990; Kao, Chen et al. 1995), and rhodamine B (Weinberg 1988), have also been used in transport experiments. A natural advantage of these labels is the avoidance of radioactivity. Techniques using nonradioactive markers have often been complicated by endogenous artifacts and the lack of standard curves to convert measured quantities to macromolecular concentrations. These markers may also cause the transport of the labeled macromolecule to differ significantly from the transport of an unlabeled molecule. This effect is thought to be negligible when a label is relatively smaller than the compound it is attached to.

The benefits of using a nonradioactive technique to quantify vascular distributions was demonstrated with the development of a technique using horseradish peroxidase (HRP), a 40 kD macromolecule, in the rat aorta (Penn, Koelle et al. 1990). This method utilized the discovery that transmission of light through tissue containing the peroxidase reaction product was found to be a predictable function of the concentration of the peroxidase present. Optical magnification provided spatial resolution superior to measuring profiles of radiolabeled macromolecules by serially sectioning tissues parallel to the intimal surface. Another benefit was that by fixing exogenous HRP *in situ*, cellular and structural features of the tissue were preserved. This technique allowed many important pharmacokinetic results to be elucidated such as the effect of endothelial cell injury on the *in vivo* transport of HRP into the aorta (Penn and Chisolm 1991) and the

permeability of the endothelium and internal elastic lamina (Penn, Saidel et al. 1994). These studies examined the transport of HRP and it was suggested similar studies could be done with other macromolecules linked to HRP, but the molecular size of HRP is comparable to many biologically significant plasma proteins such as albumin (67 kD). The aqueous tissue processing required to create the reaction product may also cause post-experiment diffusion of soluble macromolecules.

A description of the fluorescence process is necessary before discussing fluorescent labels and detection techniques. Fluorescence is the emission of energy by certain molecules after excitation by an external light source. Molecules possessing this property are called fluorescent labels or fluorophores. This process is different from chemiluminescence, where the excited state is the result of a chemical reaction. Energy from an external source such as an incandescent lamp or a laser is absorbed by the fluorophore causing it to reach an excited electronic singlet state. The molecule remains in this excited state for a finite time ($\sim 1-10$ ns) and after some energy dissipation, may reach a relaxed singlet excited state, emit a photon of energy, and return to its ground state. The energy dissipation during the excited-state lifetime decreases the energy, therefore increasing the wavelength, of the released photon compared to the incident photon. The released photon is measured usually by either a fluorescent microscope for nonaqueous phase samples or a spectrofluorometer for bulk phase samples.

Another fluorescent technique which may be used separately or in conjunction with other techniques is immunohistochemistry, the attachment of fluorescent antibodies to the compound of interest during post-experimental aqueous processing. Fluorescent signals can be amplified by repeating the aqueous processing with secondary and tertiary antibodies that attach to previously attached antibodies. This amplification allows detection of very small drug concentrations. Rigorous immobilization of exogenous compounds in the tissue is needed to prevent soluble compounds to be displaced and possibly washed away during aqueous processing.

Many different fluorescent tags are used in transport studies with the most common perhaps being fluorescein isothiocyanate (FITC), a small (389 D), neutral and polycyclic molecule that is maximally excited at 492 nm and emits energy above 530 nm. The small molecular size of FITC and the potential for spatial resolution similar to HRP studies suggest that this marker would be ideal for vascular transport studies. However, quantitative fluorescence microscopy has been hindered in the past by complications such as autofluorescence and the proper conversion of measured fluorescent intensities to physical concentrations.

II.D. Issues with Quantitative Fluorescence Microscopy

Fluorescence microscopy has desirable properties for use in quantifying compounds in vascular tissue such as providing multi-dimensional information, high spatial resolution and not depending on aqueous processing. However, autofluorescence and the proper conversion of fluorescent intensity from fluorophores to physical concentrations of the compound of interest have limited the use of fluorescence microscopy in quantitative studies. A review of recent studies which have utilized advances in computers, digital processing and microscopy suggest that these complications can be correctly compensated for.

II.D.1. Autofluorescence

Autofluorescence is the phenomena wherein endogenous molecules emit energy in the same frequency region as introduced fluorescent labels thereby obstructing view of these labels. The autofluorescence of biomolecules such as elastin, fibronectin and lipofuscin have been found to be sufficiently broadband and cannot be avoided by selecting a fluorescent probe with excitation and emission spectra outside the range of autofluorescent molecules because these spectra are often very broad. Autofluorescence may be very intense, masking the fluorescent signals of interest. The inhomogeneity of

tissues and autofluorescent molecules often cause this artifact to be highly nonuniform and difficult to compensate for.

The few reports for reducing or eliminating autofluorescence principally apply to flow cytometry studies. Different strategies have been suggested to compensate for the autofluorescence in fluorescence microscopy studies with no standard being adopted. One strategy that has been used in histological preparations involves counterstaining the specimen with another compound to quench or absorb the autofluorescence. Crystal violet has an absorption spectrum that overlaps with the emission spectrum of some autofluorescent molecules and has been used to quench autofluorescence (Halldén, Sköld et al. 1991; Kong and Ringer 1995), but this technique is not adaptable to fluorescence microscopy studies.

Time-resolved fluorometry, which utilize the different decay times of autofluorescent molecules and fluorescent tags, has also been used to compensate for autofluorescence (Koppel, Carlson et al. 1989). This technique often requires a sophisticated fluorescence microscope to visualize the time-resolved emission and a marker such as fluorescent lanthanide chelates which has a long decay time (Seveus, Väisälä et al. 1992). The high cost of the required microscope system and the scarcity of compounds of interest that are conjugated to these probes may make this method impractical.

Digital image processing methods have been proposed to reduce and/or eliminate autofluorescence, first in flow cytometry studies (Steinkamp and Stewart 1986) and then in histological preparations (van de Lest, Versteg et al. 1995). These post-processing algorithms were developed after the observation that fluorescent labels have narrower excitation and emission spectra than the endogenous compounds responsible for autofluorescence. The autofluorescence at different wavelengths are correlated with each other and this correlation is used in combination with an image at one wavelength containing only autofluorescence to estimate the autofluorescence in a corresponding

image at a different wavelength containing both autofluorescence and the signal of interest from fluorescent markers. The estimated autofluorescence can then be subtracted from the original image to yield an image whose autofluorescence has been reduced or eliminated. One advantage of this technique is that a standard fluorescence microscope with different filter sets is more cost-effective than a microscope with time-delayed fluorometry capability.

II.D.2. Conversion of Intensities to Concentrations

Fluorescent microscopy is usually used as a binary tool to determine the presence or absence of a compound by qualitatively assessing the fluorescence from markers attached to the compound of interest. This method is feasible only if the emitted fluorescence is much brighter than background. The relation between the fluorescent intensity from fluorescent tags and the physical concentration of the complex that the tag is conjugated to is often not quantified. Quantitative analysis requires the development of a reliable calibration curve to convert fluorescent intensities to physical concentrations of the compound the label is attached to. The development of an appropriate standard curve to accomplish this is often the major difficulty when attempting to perform quantitative fluorescence microscopy. The intensity of various concentrations of a FITC solution in a hemocytometer (Nakamura and Wayland 1975; Fox and Wayland 1979) or capillary tubes (Nugent and Jain 1984) has been used to construct a calibration curve. These techniques have been questioned because the difference in thickness of a section of tissue compared to a hemocytometer or capillary tube may cause calculated tissue concentrations to not accurately represent the actual tissue concentration (Armenante, Kim et al. 1991).

II.E. Chapter Summary

Advances in biological and medical research have led to identification of a variety of compounds that may be of therapeutic value. The administration of these agents is not straightforward, originally complicated by narrow therapeutic ranges and quick

degradation and clearance. Consistent, sustained release devices remedied these problems, but further improvements can only be gained by understanding the transport and deposition within the arterial wall. Current techniques used to assess macromolecular distributions within the heterogeneous arterial wall have been limited by low spatial resolution and post-experiment artifact. A new technique to quantitatively assess vascular drug distributions is needed along with more experimentation to elucidate macromolecular transport within vessels. Fluorescence microscopy has many desirable properties for quantifying compounds in tissue, but has not been used previously mainly due to autofluorescence and difficulties converting fluorescent intensities to physical concentrations. There appear to be methods to handle these issues and make quantitative fluorescence microscopy the high resolution technique necessary for future investigation of macromolecular transport within vascular tissue.

III. Quantification of Macromolecular Distributions in Vascular Tissue

III.A. Introduction

Various mathematical models have been developed to describe macromolecular pharmacokinetics in the vessel wall (Fry 1985; Saidel, Morris et al. 1987; Penn, Saidel et al. 1992). The insight gained from these models is directly related to the arterial concentration profiles used to estimate transport parameters in a model. Current techniques to quantify macromolecular distributions are inadequate and suggest that new techniques need to be developed. The limited spatial resolution of some methods forces characterization of deposition to general, homogeneous compartments which conceals local concentration gradients in the vessel wall. Other techniques have been complicated by post-experimental artifact and low signal-to-noise ratios. High resolution concentration profiles will lead to better pharmacokinetic models and improved understanding of macromolecular transport and deposition in vascular tissue.

A new method has been developed for visualizing and quantifying macromolecular distributions in vascular tissue. This technique utilizes fluorescence microscopy with digital post processing, and avoids the experimental and disposal hazards involved with radiolabeled compounds while providing spatial resolution comparable to conventional radioactive techniques. A non-aqueous method to immobilize drug is used to prevent post-experimental diffusion of soluble molecules, a complication of some previous techniques. Vessel cross-sections are imaged with fluorescence microscopy, and digital post processing algorithms are used to reduce autofluorescence, the main complication of quantitative fluorescence microscopy. Autofluorescence compensation is accomplished by using images acquired at two different excitation wavelengths, one image containing both the fluorescence of markers and autofluorescence, and the other image containing only autofluorescence. The latter image is then used to estimate the autofluorescence in

the former image. This estimated autofluorescence can then be subtracted from the former image to yield an autofluorescence-free image containing only the signal from the fluorescent tags. Fluorescent intensities are then converted to tissue concentrations after autofluorescence compensation, yielding a two-dimensional, high resolution macromolecular distribution within a vessel cross-section. A demonstration of this technique examining the transvascular transport of dextrans in the calf carotid artery is shown. This technique can be used to investigate the pharmacokinetics of different compounds to provide the quantitative data necessary to evaluate transport models and gain insight into the transport of administered agents as well as elucidate details of blood vessel physiology, homeostasis, and pathology.

III.B. Materials and Methods

III.B.1. Calibration Standards

Calf carotid arteries were obtained from a slaughterhouse (Research 87) and stored on ice for no more than two hours. The arteries were placed in phosphate buffer saline with calcium and magnesium (PBS⁺⁺) throughout the preparation process to prevent dehydration and maintain tissue viability. Excess fascia and fat was gently teased away using forceps and scissors prior to sectioning vessels into cylindrical rings, 8-12 mm long and 4-8 mm in diameter. These rings were placed into separate vials containing 10 ml of known concentrations of 20 kD dextrans labeled with fluorescein isothiocyanate (FITC-Dx, 0.006-0.007 mol FITC per mol glucose, Sigma) in PBS⁺⁺. Control specimens were incubated in 10 ml PBS⁺⁺ without any FITC-Dx. The vials were wrapped with aluminum foil to prevent photobleaching of the fluorescent labels from extraneous light, and incubated at 4° C in the dark for 24 hours before immobilization.

III.B.2. Immobilization and Sectioning

Tissues were snap frozen immediately after removal from an incubation vial. Arteries were placed in plastic molds (Polysciences) and oriented for future sectioning with forceps. The mold was then filled with embedding medium (O.C.T., Tissue-Tek) and placed in a bath of liquid nitrogen to solidify the medium. Specimen blocks were stored at -20 °C prior to being cut into 20 μm thick cross-sections using a precooled cryostat (Ames Cryostat II, Miles). Frozen medium around the tissue was gently removed to facilitate mounting onto slides. Specimens were transferred onto glass slides (Superfrost Plus, VWR Scientific), freeze dried at -50 °C in a lyophilizer (Labconco) for 24 hours, and stored at room temperature in a dark, dry environment until imaging.

III.B.3. Image Acquisition System

24-bit color images were acquired using a CCD video camera system (Optronics) attached to a fluorescence microscope (Optiphot-2, Nikon). The system resided on a pneumatic optical table (Technical Manufacturing Corporation) to minimize vibrations. Video images were captured on a computer (Power Computing) via a frame grabber (LG-3, Scion) using a commercial imaging software package (IPLab Spectrum, Signal Analytics). The frame grabber was calibrated by displaying a test image consisting of color bars generated from the video camera system. The gain and offset of the frame grabber were adjusted to match its dynamic range (0 to 255 units for the red, green and blue channels) to the dynamic range of the video camera system. Magnification was provided by a x10 ocular and a x10 objective, resulting in 640 by 480 pixel images with pixel dimensions of 1.326 μm by 1.326 μm . Illumination was provided by a super high pressure mercury lamp (Nikon) which was allowed to warm up for at least 2 hours prior to imaging for consistent illumination. The duration needed for the lamp to stabilize was determined by imaging a blank slide at various intervals after the system was turned on. The mean intensity of a 51 by 51 pixel region in the center of the image was found to stabilize after 2 hours. UV and FITC filter sets were used to examine tissue specimens.

The UV filter set consisted of an excitation filter of 330-380 nm, a dichroic filter (beamsplitter) of 400 nm and a barrier filter of 420 nm, and the FITC filter set consisted of an excitation filter of 465-495 nm, a dichroic filter of 505 nm and a barrier filter of 515-555 nm. The fluorescent tag used in these experiments, fluorescein isothiocyanate (FITC), is maximally excited around 490 nm so UV images contain only autofluorescence and FITC images contain both autofluorescence and signal from the fluorescent labels. Hence forth, UV and FITC images refer to images taken with the UV and FITC filter sets, respectively.

III.B.4. Initial Processing

Images were acquired using RGB (red, green, blue) color components and converted to the HSV (hue, saturation, value) color model. The HSV color model decouples intensity from color information in an image, with the value image containing intensity and the hue and saturation images containing color information. Both UV and FITC images were decoupled in this manner and the hue and saturation images were discarded (step 1 in Figure 2). The remaining intensity value image has intensity values range from 0 (absolute black) to 255 (absolute white).

This study focused on obtaining concentration profiles across the media, the middle layer of the artery between the intima and adventitia, since many vasotherapeutic compounds target smooth muscle cells in the media. Similar processing can be used to examine other layers of the artery. A 51 pixel wide region of each image was selected for analysis that spanned across the media (step 2 in Figure 2). Hence forth, UV and FITC regions will refer to the extracted region corresponding to the media in the UV and FITC images, respectively. These regions were then corrected for autofluorescence.

III.B.5. Autofluorescence Compensation

Since UV images contain only autofluorescence and FITC images contain both autofluorescence and the signal of interest, each pixel in a UV image can be used to

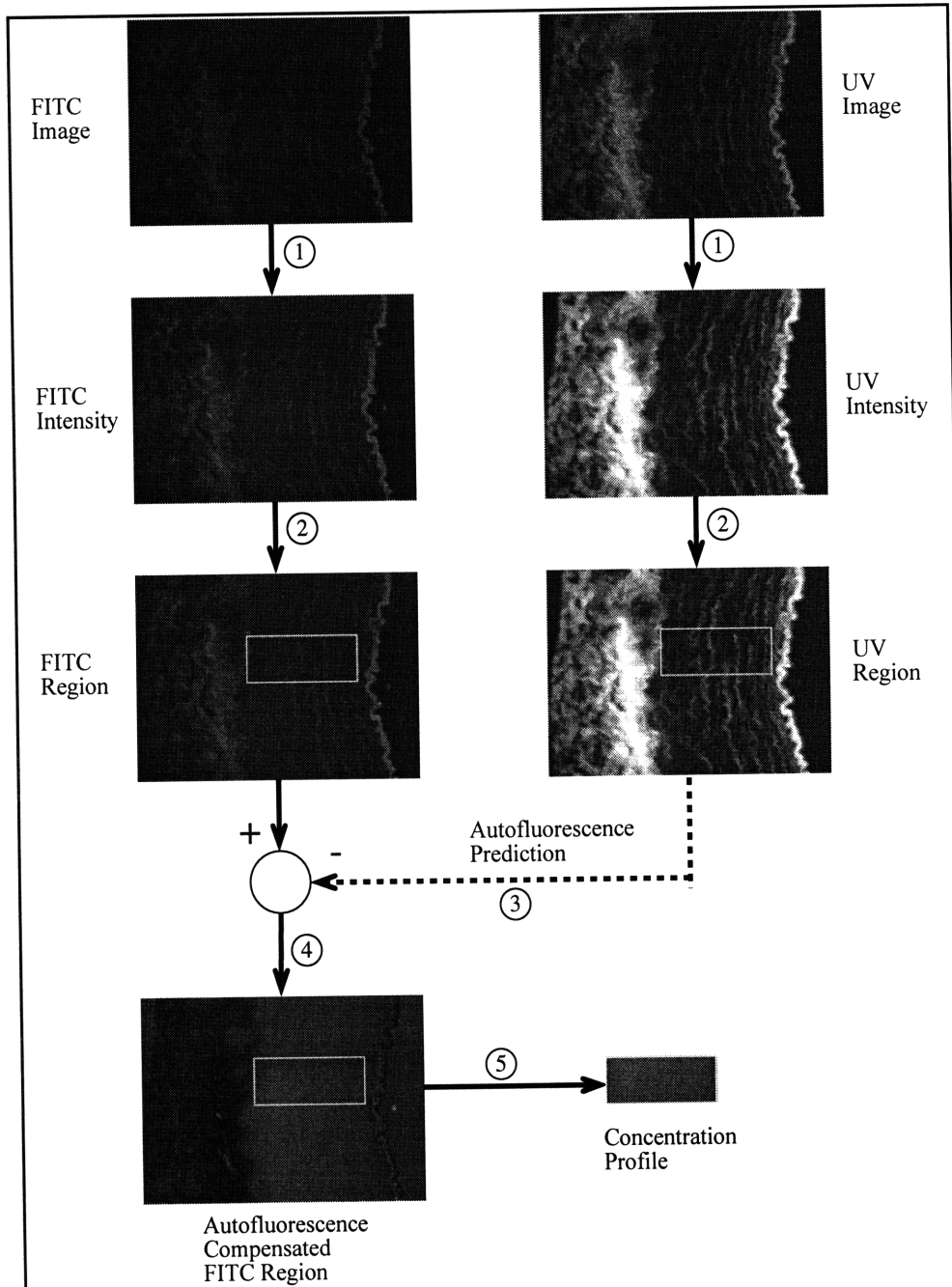


Figure 2. Post processing algorithm to compute concentration profiles. The top two color images are fluorescent images of a cross-section of a calf carotid artery imaged with the FITC and UV filter sets, respectively. (1) The intensity subimage of each color image is extracted. (2) A region corresponding to the media is extracted from each intensity subimage. (3) The UV region is used to estimate autofluorescence in the FITC region. (4) The estimated FITC autofluorescence is subtracted from the FITC region, yielding only the signal from fluorescent labels. (5) Pixel intensities are converted to tissue concentrations resulting in a two-dimensional concentration profile of fluorescent labeled compounds within the tissue.

estimate the autofluorescence in the corresponding pixel in the counterpart FITC image. Corresponding pixels from the UV and FITC regions of a control specimen were correlated, yielding a relationship which allows the estimation of the autofluorescence component in each pixel of a FITC region using the corresponding pixel in the counterpart UV region (step 3 in Figure 2). This estimated autofluorescence is then subtracted from the original FITC image yielding an autofluorescence compensated FITC image that contains only the signal from fluorescent markers (step 4 in Figure 2).

III.B.6. Conversion of Fluorescent Intensities to Tissue Concentrations

Fluorescent intensities were converted to tissue concentrations using a standard curve obtained from specimens incubated until equilibrium in known concentrations of FITC-Dx in PBS⁺⁺. The average fluorescent signal in an autofluorescence compensated FITC region of a specimen was correlated with the bulk phase concentration of FITC-Dx in PBS⁺⁺ the specimen was incubated in. This allowed fluorescent intensities to be converted to bulk phase concentrations. Compounds in bulk solutions are free to access any portion of a unit volume of solution. In contrast, compounds in tissue are excluded from certain regions of a unit volume by steric interactions. The volume accessible is a fraction of the total tissue volume and this fractional tissue volume is needed to convert bulk phase concentrations to tissue concentrations. An independent measurement correlating bulk phase concentrations and tissue concentrations gives the fractional volume of the tissue available for compound distribution. The two previous relations can then be combined to convert the fluorescent intensity of every pixel in an autofluorescence compensated FITC images to a tissue concentration of FITC-Dx in PBS⁺⁺ (step 5 in Figure 2). Applying this relation to the autofluorescence compensated FITC region yields a two-dimensional concentration profile of the vessel cross-section.

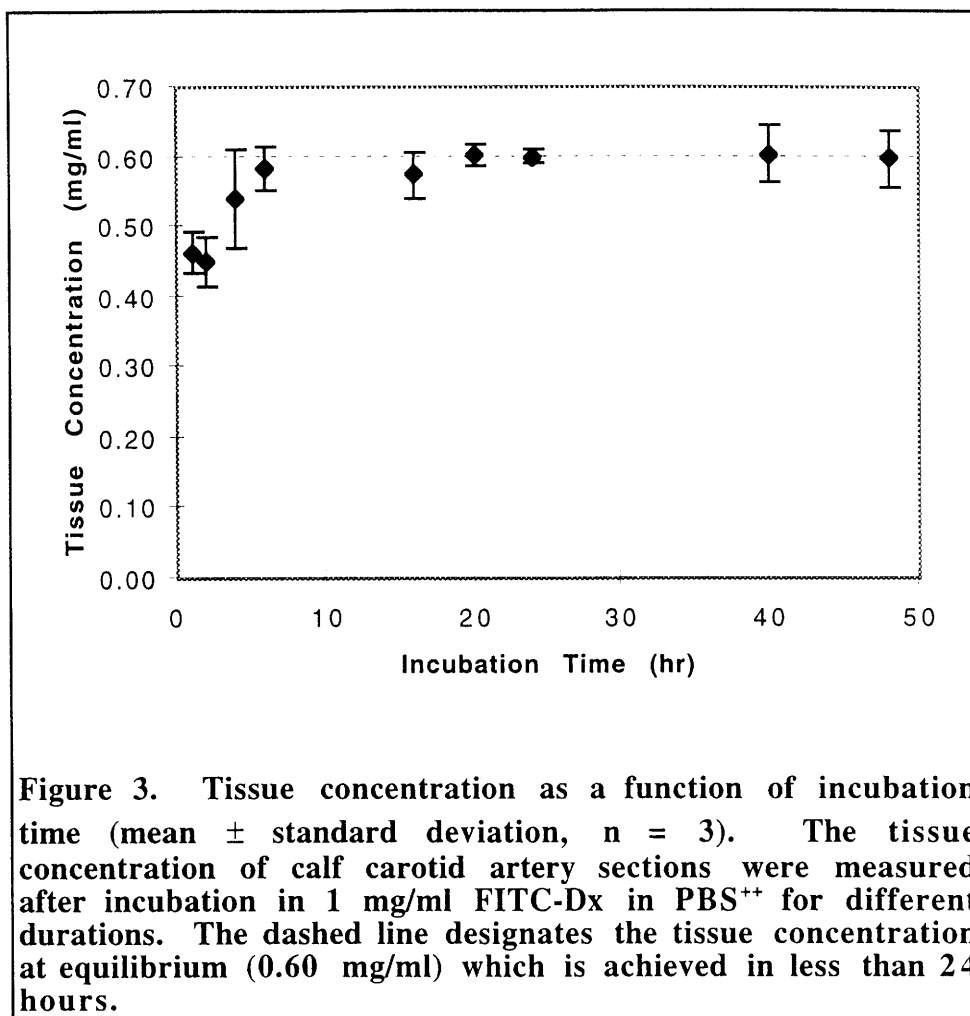
III.B.7. Equilibrium Time for Standards

The use of calibration standards to convert fluorescent intensities to drug concentrations requires standards that are incubated until the tissue is at equilibrium with the bulk incubation solution. The incubation time required for standards to reach equilibrium was determined by incubating cylindrical segments of calf carotid arteries in 10 ml of 1 mg/ml FITC-Dx in PBS⁺⁺ at 4° C for durations ranging from 1 hour to 48 hours. After the incubation period, each tissue section was blotted to remove adsorbed solution, weighed wet and reincubated in 10 ml of fresh PBS⁺⁺ at 4° C for 48 hours to allow the drug to diffuse out of the tissue. Samples of the reincubation solution were measured with a spectrofluorimeter (Fluorolog 1681, SPEX). The resulting fluorometric counts per second were converted to bulk solution concentrations using a standard curve created with known concentrations of FITC-Dx in PBS⁺⁺.

This bulk phase reincubation concentration of FITC-Dx in PBS⁺⁺ (C_2) can then be used to calculate the original tissue concentration of FITC-Dx in PBS⁺⁺ (C_T) with the following formula which is derived in the Appendix:

$$C_T \approx \frac{C_2 V \rho}{x}$$

where V is the volume of the reincubation bath volume, ρ is the density of tissue, and x is the wet tissue weight. In separate experiments, the density of calf carotid arteries (ρ) was measured to be 1.07 ± 0.096 mg/ml ($n=15$) using a micro-graduated cylinder and an analytical balance. It was determined that 24 hours was sufficient for the tissue sections to reach equilibrium with the FITC-Dx solution (Figure 3).



III.B.8. Demonstration

To demonstrate the utility of this technique, arterial concentration profiles were constructed from calf carotid arteries that were placed in an *in vitro* perfusion apparatus designed to simulate plasma flow. A schematic diagram of the apparatus is illustrated in Figure 4. Excess fascia and fat from calf carotid arteries were removed as described in the Materials and Methods section and artery segments without visible branches were then cannulated at both ends and tested for leaks by visually inspecting the vessel after connecting one end to an elevated Ringer's solution source and closing off the other end. Intact arteries were then placed in a perfusion apparatus which has separate endovascular and perivascular compartments which allow establishment of a transvascular

concentration gradient. Arteries were perfused with an endovascular bath of 1 mg/ml FITC-Dx in PBS⁺⁺ and a perivascular bath of PBS⁺⁺ at room temperature. There was no transvascular pressure gradient across the vessel, so any transport would be due solely due to diffusion. Specimens were immediately snap frozen, sectioned, imaged, and digitally post processed as described previously. Vessel cross-sections were oriented during imaging so that regions could be extracted which could be averaged across each column to obtain a transvascular concentration profile.

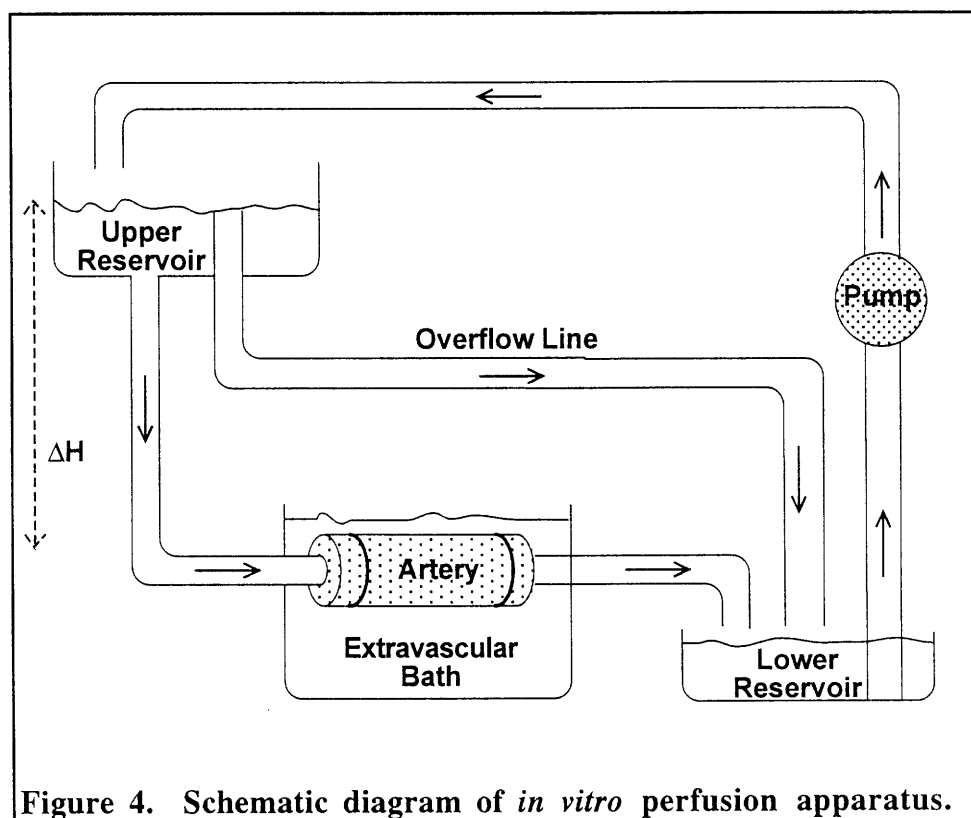


Figure 4. Schematic diagram of *in vitro* perfusion apparatus.

III.C. Results

III.C.1. Autofluorescence Compensation

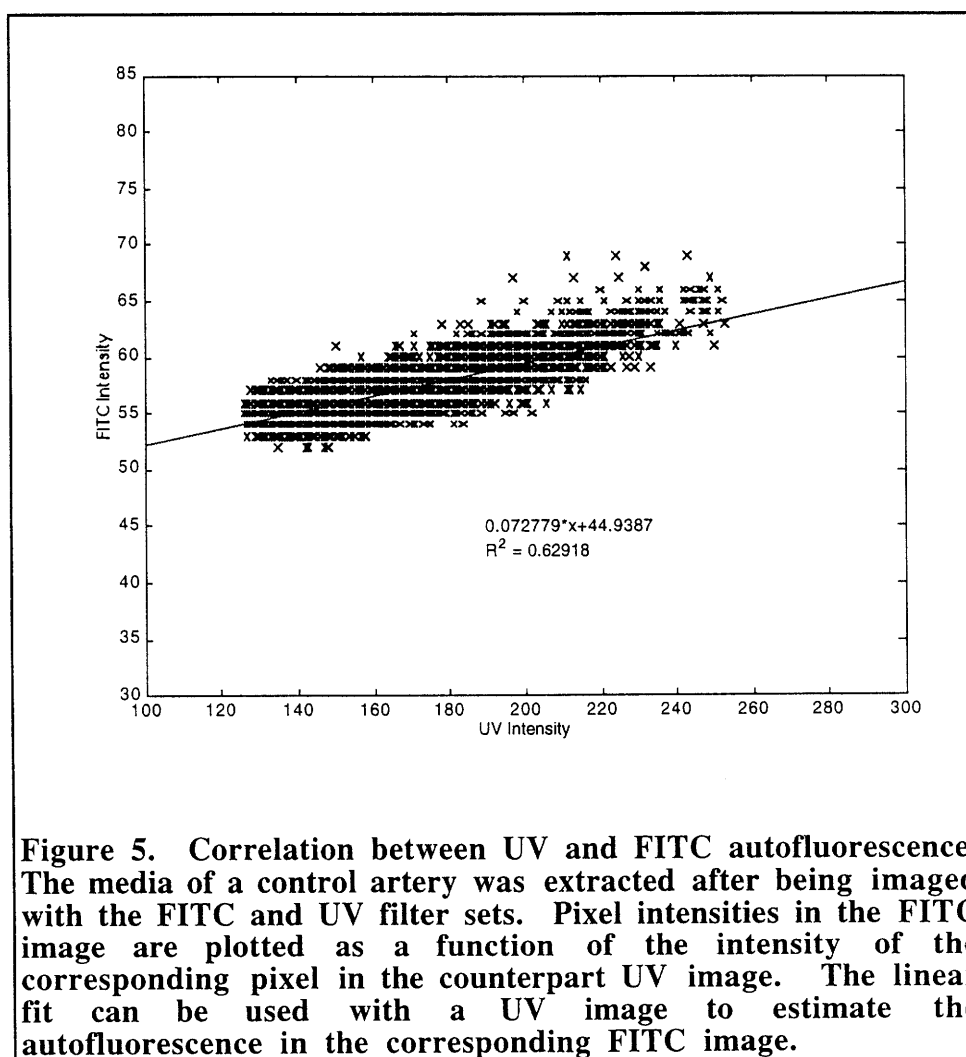
UV and FITC images of control arteries were examined to correlate the autofluorescence at the UV and FITC wavelengths. Figure 5 shows a scatter diagram of

pixel intensities in a UV region of a control artery versus the corresponding pixel intensities in the FITC region along with a linear fit to the intensities. The linear relationship allows the estimation of the autofluorescence component in each pixel of other FITC images using the corresponding pixel in the counterpart UV image:

$$FITC(\text{autofluorescence}) = A * UV(\text{total}) + B$$

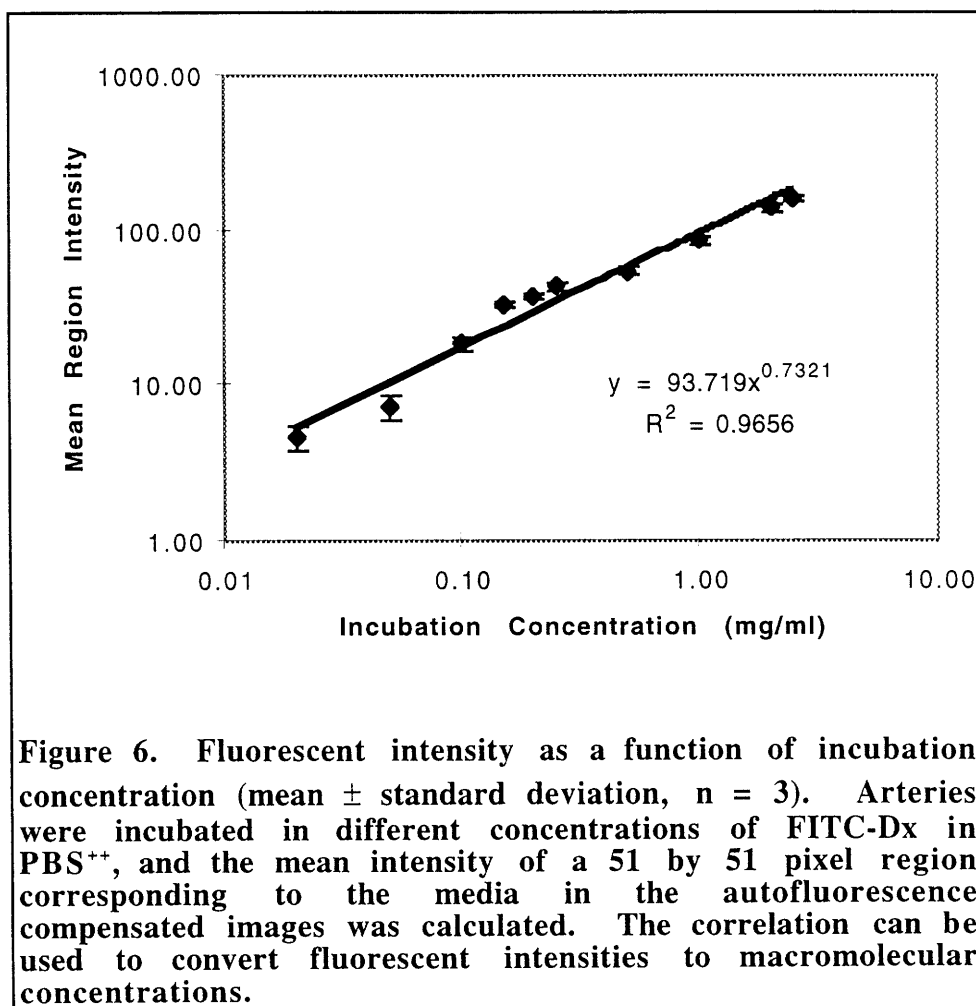
where $A = 0.073$ and $B = 44.94$. The estimated autofluorescence can then be subtracted from the original FITC image yielding the signal of fluorescence markers alone:

$$\begin{aligned} FITC(\text{specific}) &= FITC(\text{total}) - FITC(\text{autofluorescence}) \\ &= FITC(\text{total}) - (A * UV(\text{total}) + B) \end{aligned}$$



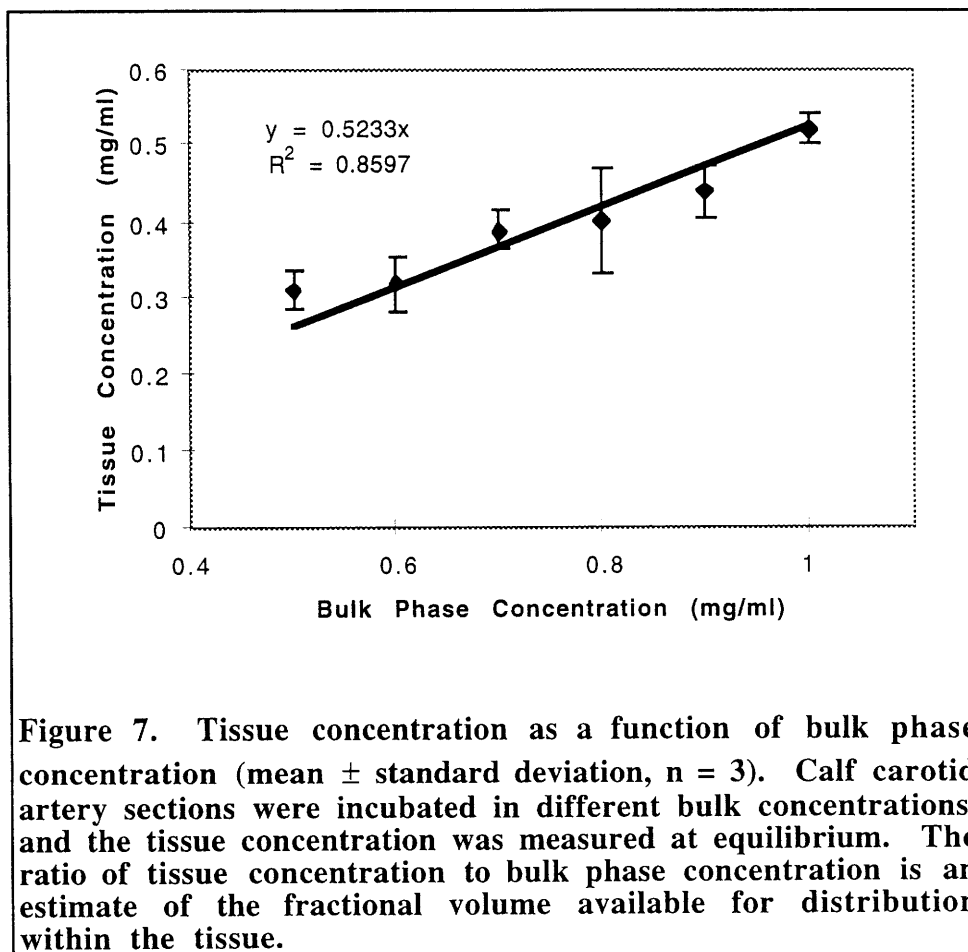
III.C.2. Conversion of Fluorescent Intensities to Tissue Concentrations

The conversion of fluorescent intensities to tissue concentrations requires two relations. The first is the relation between fluorescent intensities and bulk phase concentrations of calibration standards, specimens incubated until equilibrium in known concentrations. The range of this mapping is bounded by two factors. The lower concentration bound is determined by the sensitivity of the image acquisition system, and low fluorescent emissions from dilute concentrations of the fluorescently labeled drug. The upper concentration bound is determined by saturation of the image acquisition system. Figure 6 shows the mean region intensity plotted versus the bulk phase incubation concentrations of FITC-Dx in PBS⁺⁺ and a semilog curve fit to the data.



As described above, autofluorescence was compensated before constructing this relationship. The data show that bulk phase concentrations ranging over two orders of magnitude (0.02 mg/ml to 2.5 mg/ml) can be reconstructed by inverting the curve fit to the data.

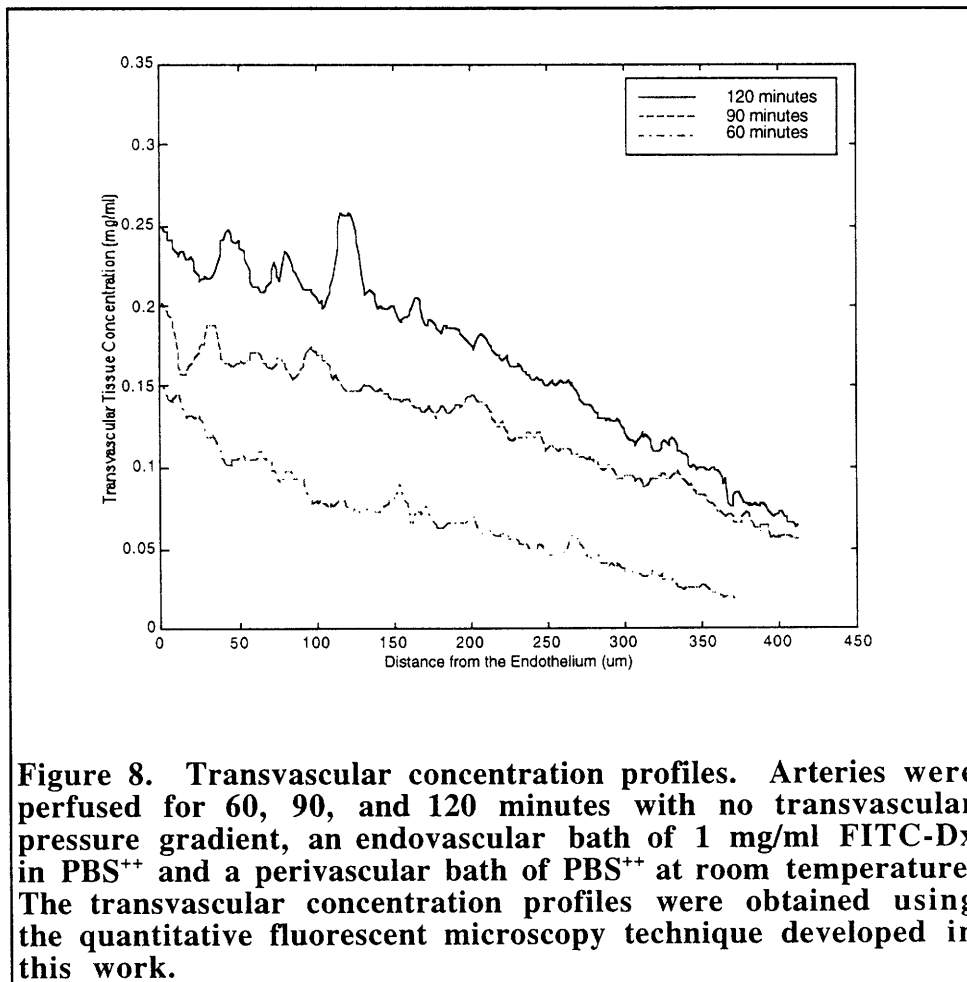
The second relation needed to convert fluorescent intensities to tissue concentrations is the fraction of tissue volume available to a compound. The fractional tissue volume was determined by examining cylindrical sections of calf carotid arteries incubated in 10 ml of different concentrations of FITC-Dx in PBS⁺⁺ for 24 hours. As shown earlier, this time is sufficient to reach equilibrium (Figure 3). Tissue concentrations were computed as described in the Appendix. Figure 7 shows tissue concentration plotted versus bulk phase concentrations of FITC-Dx in PBS⁺⁺ in calibrations samples that were incubated from 0.5 mg/ml to 1 mg/ml.



The slope of the linear correlation between bulk phase and tissue concentrations is the fractional tissue volume available to FITC-Dx. This fractional volume allows bulk phase concentration to be converted to tissue concentrations.

III.C.3. Demonstration

Figure 8 shows transvascular concentration profiles obtained for arteries that were perfused for 60, 90, and 120 minutes with no transvascular pressure gradient, an endovascular bath of 1 mg/ml FITC-Dx in PBS⁺⁺ and a perivascular bath of PBS⁺⁺ at room temperature. A one-dimensional transvascular profile was obtained by averaging across the width of the two-dimensional FITC region obtained after applying the post processing algorithm described earlier.



III.D. Discussion

A new technique has been developed to obtain arterial concentration profiles combining fluorescence microscopy and post processing. The use of fluorescence microscopy offers several advantages over other techniques that have been developed to quantify arterial concentrations of compounds, but also introduces additional issues such as autofluorescence and the conversion of fluorescent intensities to physical concentrations.

III.D.1. Comparison with Other Techniques

Vascular deposition studies have utilized radioactive nuclides which minimally change the physical structure of a compound and its transport properties, but these experiments often have limited spatial resolution and experimental and disposal hazards. Early studies measured the radioactivity in manually dissected sections providing questionable repeatability as well as limited spatial resolution (Duncan, Buck et al. 1963). Measuring radioactivity in *en face* serial sections, sections parallel to the intimal surface, provides resolution of 10-20 μm and can only assess the macromolecular distribution in one orientation (Bell, Adamson et al. 1974; Bell, Gallus et al. 1974; Bratzler, Chisolm et al. 1977; Bratzler, Chisolm et al. 1977; Ramirez, Colton et al. 1984; Tedgui, Merval et al. 1992). The radiolabeled drug content in a specimen can also be visualized by allowing the specimen to develop specially prepared photographic film or an emulsion silver preparation. The density of exposed silver grains can then be quantified by silver grain counting or optical density methods. These autoradiographic techniques offer increased resolution (up to $\sim 2 \mu\text{m}$), but may be hampered by inaccurate localization, the grain size of the photographic film, inconsistent background radiation and/or post-experimental diffusion of soluble macromolecules in the emulsion silver preparation (Aitken, Wright et al. 1968; Fry, Mahley et al. 1980; Schnitzer, Morrel et al. 1987; Tompkins, Yarmush et al. 1989). The duration needed to expose the developing film or emulsion preparation may also be inconvenient.

Nonisotopic techniques include biochemical and fluorescent labels. They offer higher spatial resolution and avoid the hazards of radioactivity, but may be limited by marker sizes, which affect the physicochemical properties of labeled macromolecules. The transport of horseradish peroxidase (HRP) has been quantified in arteries using a colored reaction product whose intensity was a function of the concentration of HRP (Penn, Koelle et al. 1990). Specimens were examined with a light microscope which provided HRP concentration profiles with spatial resolution superior to radioactive techniques. Similar studies with vasoactive compounds would greatly aid drug delivery research, however, this technique has not been adapted to study vasoactive compounds. The large size of HRP (40 kD) prevents its utility as a molecular tag on much smaller drugs. In addition, the aqueous tissue processing required to create the colored reaction product may also cause post-experiment diffusion. Fluorescence microscopy offers the advantage of obtaining high spatial resolution data as in HRP studies, using smaller sized marker (e.g. the common fluorescent tags, FITC and rhodamine isothiocyanate, are ~400 D) and does not require aqueous tissue processing. Quantitative studies, however, have been complicated by autofluorescence and the proper conversion of fluorescent intensities and drug concentrations. However, methods have been developed to minimize these complications.

III.D.2. Autofluorescence Compensation

Constituent arterial components such as elastin, fibronectin and lipofuscin, exhibit autofluorescence, the emission of energy in the same frequency region as exogenous fluorescent labels (van de Lest, Versteeg et al. 1995). The fluorescence spectra of these compounds are very broad and the autofluorescence cannot be avoided by selecting a probe with excitation and emission spectra outside their range. Autofluorescence may be very intense, masking the fluorescent signals of interest and the inhomogeneous distribution of autofluorescent molecules often cause this artifact to be nonuniform and difficult to compensate for. Attempts to eliminate background autofluorescence by

counterstaining connective tissue with compounds such as crystal violet (Halldén, Sköld et al. 1991) or pontamine sky blue (Cowen, Haven et al. 1985) derived from flow cytometry applications may not be suitable because such aqueous tissue processing may result in post-experimental diffusion of the drugs.

Time-resolved fluorometry, which utilizes the different decay times between autofluorescent molecules and fluorescent tags, has also been used to compensate for autofluorescence (Koppel, Carlson et al. 1989; Marriott, Clegg et al. 1991). In addition to requiring a sophisticated fluorescence microscopy system, this technique may require special fluorescent tags such as lanthanide chelates (Seveus, Väisälä et al. 1992), which may not be readily available individually or conjugated to compounds of interest.

After the observation that fluorescent labels have narrower excitation and emission spectra than the endogenous compounds responsible for autofluorescence, digital image processing methods have been developed to reduce and/or eliminate autofluorescence, in flow cytometry studies (Steinkamp and Stewart 1986) and in histological preparations (Szöllösi, Lockett et al. 1995; van de Lest, Versteg et al. 1995). Images were captured at two wavelengths with one image consisting only of autofluorescence, and the other image possessing both autofluorescence and the fluorescence signal of interest. The former image is then be used to estimate the autofluorescence in the latter image. Assuming that autofluorescence and the fluorescence from the labels are simply additive components, the estimated autofluorescence is then subtracted from the latter image to yield an autofluorescence compensated image with signal only from the fluorescent probes. The main advantage of this technique is that it is simple to implement. A disadvantage of this technique is that different tissue types may need to be compensated separately because the function used to estimate the autofluorescence at one wavelength using the autofluorescence of another wavelength is probably different for different tissues.

III.D.3. Conversion of Fluorescent Intensities to Tissue Concentrations

Fluorescent microscopy is usually used as a binary tool to determine the presence or absence of a compound by qualitatively assessing the fluorescence from markers attached to the compound of interest. The relation between the fluorescent intensity from fluorescent tags and the tissue concentration of the compound that the tag is conjugated to is often not quantified. Quantitative analysis requires the development of a reliable calibration curve to convert fluorescent intensities to physical concentrations. Calibration curves have been constructed by measuring the intensity of various concentrations of a FITC solution in a hemocytometer (Nakamura and Wayland 1975; Fox and Wayland 1979) or capillary tubes (Nugent and Jain 1984) to obtain a calibration curve. As pointed out by Armenante et al. (1991), the difference in thickness of a section of tissue compared to a hemocytometer or capillary tube may cause calculated tissue concentrations to not accurately represent the actual tissue concentration. To date, there has been no attempt to create standard curves for fluorescent compounds in arteries using the identical tissue for both experimentation and calibration. This was accomplished in this study by incubating tissue in different concentrations until equilibrium. These calibration standards were then used to construct a relationship between fluorescent intensity and bulk phase concentration. Bulk phase concentration can then be converted to tissue concentration by measuring the fractional volume available to the particular compound.

III.D.4. Future Applications

The examples shown here demonstrate the potential of this technique for providing high resolution concentration profiles. Note that higher magnification could have been used for higher spatial resolution, but this magnification allows the entire width of a calf carotid artery to be captured onto a single image. Since this technique is adaptable to studies with different compounds, one could perform similar studies with compounds of slightly differing physicochemical properties. These studies would show

the relative importance of physicochemical properties such as size, charge, solubility, and flexibility on the transport and deposition of compounds through the arterial wall. Dextrans would be ideal for these experiments since fluorescently labeled dextrans are readily available with different molecular weights. Amino and sulfide groups could also be conjugated to examine the effect of charge on transport. By combining data from these experiments, a model could be constructed to predict the transport of a compound based solely on its physicochemical properties.

III.E. Chapter Summary

Biomedical research continues to elucidate details about the pathobiology of many diseases leading to the development of new therapeutic agents. The therapeutic potential of these pharmacological agents has been confounded by an inability to describe macromolecular distributions within the heterogeneous arterial wall which has led to inadequate understanding and modeling of the pharmacokinetics of compounds following administration. Quantitative tools to assess vascular distributions of macromolecules need to be developed to provide high spatial resolution distribution profiles. These profiles will allow quantitative pharmacokinetic models to be evaluated, resulting in improved understanding of solute transport through the vessel wall and development of better vascular pharmacokinetic models. This work describes a quantitative fluorescence microscopy technique which is made possible by digital post processing to eliminate autofluorescence and convert fluorescent intensities to drug concentrations. This technique offers spatial resolution comparable to conventional radioactive techniques and is adaptable to fit many experimental protocols. In addition to aiding the evaluation and rational design of drug delivery strategies, this technique can be a valuable tool for investigation into the pharmacology and physiology of the vessel wall.

IV. Measurement of Transvascular Transport Parameters

IV.A. Introduction

A new method utilizing quantitative fluorescence microscopy with digital post processing to measure vascular tissue concentrations was described in the last chapter. This technique was developed after determining that previous methods used to assess vascular distributions were inadequate for studying macromolecular transport in the vessel wall. This chapter describes the integration of this new technique with *in vitro* experiments and mathematical modeling to estimate transport parameters such as effective diffusivity, convective velocity and endothelial permeability. These transport parameters can then be used to construct detailed mathematical models that predict macromolecular distributions under different conditions. These models will be of great utility to drug delivery research as they provide a method to test the feasibility and efficiency of different drug delivery schemes without actually performing *in vivo* experiments.

The transport of 20 kD dextrans (polymers constructed using a glucose monomer) labeled with fluorescein isothiocyanate (FITC) in calf carotid arteries were examined in an *in vitro* perfusion apparatus which simulates plasma flow. These experiments were performed for different durations with varying transvascular pressure and concentration gradients. Perfused arteries were processed using the technique developed in the previous chapter. Arterial concentration profiles are extracted from the fluorescence microscopy images and fitted to a mathematical model of transvascular transport. The transport parameters obtained from these experiments can then be used to simulate the transport and deposition of 20 kD dextrans under different conditions. Preliminary results are shown to demonstrate the feasibility and potential of these proposed experiments.

Dextrans were chosen as the model compound for these studies because they are inexpensive and readily available with fluorescent tags conjugated to them. The use of

dextran is also advantageous because their physico-chemical properties are easily modifiable. For example, amino and sulfide groups can be attached to alter its charge and different sized dextrans can be obtained simply by constructing smaller or longer polymer units. Future experiments using similar dextrans could be compared to isolate the effects of different physico-chemical properties on a compound's vascular pharmacokinetics. These experiments will lead to a better understanding of solute transport and deposition in the vessel wall which can then be applied to improve drug delivery.

IV.B. Mathematical Modeling

Many different mathematical models of transvascular transport have been proposed by different investigators (Fry 1985; Saidel, Morris et al. 1987; Penn, Saidel et al. 1992). Transport studies have usually assumed circumferential and longitudinal symmetry and modeled transvascular transport due to the complex nature of multi-dimensional transport, and lack of circumferential and axial deposition data. Lumped kinetic models were developed to quantify macromolecular uptake (Duncan, Cornfield et al. 1959). In these early models, the artery and plasma are represented as individual, well mixed components with transport between them governed by first order transport kinetics. These models are limited because their empirical nature provides little insight into the mechanisms of solute transport within the artery. Another approach is to depict the arterial wall as an infinite number of concentric and infinitesimally thin homogeneous compartments (Lovich and Edelman 1996). Since these distributed or continuum models describe the tissue concentration in the vessel wall continuously, local changes in transport are evident as concentration gradients. Transport parameters are obtained by fitting measurements of arterial concentration profiles to a theoretical model of vascular transport. These parameters quantitatively describe transport within the vessel wall, and can be used to simulate the effect of different loading conditions.

The model used in this study is similar to one used to analyze dynamic transvascular macromolecular concentrations of horseradish peroxidase as a function of

time and radial distance from the internal elastic lamina (IEL) (Penn, Saidel et al. 1992). In this model, the endothelium and IEL are assumed to act as an infinitesimally thin endovascular "membrane" with transport characterized by a permeability (P_{endo}). Similarly, the adventitia is considered to be a infinitesimally thin perivascular membrane with permeability (P_{peri}). Both of these membranes can also be defined in terms of their resistance, the inverse of permeability. The model assumes the media is homogeneous and solute transport across the media is assumed to occur only by diffusion or convection. The random collision of macromolecules driven by transvascular concentration gradients results in diffusion, quantitatively described by an effective diffusivity (D). A transvascular pressure gradient and the porosity of an artery result in convection, the transport of solutes in fluids being driven across the vessel wall, characterized by a convective velocity (V). Another parameter that must be defined is the fraction of the tissue space available for macromolecular distribution (ε). (Note that $0 \leq \varepsilon \leq 1$.) This parameter allows concentrations in the model to be expressed per volume of wet tissue and defines the relation between these tissue concentrations to bulk phase concentrations (such as the endovascular and perivascular bath concentrations) which are expressed per volume accessible to a compound.

The basic equation of transvascular transport has diffusion mediated and convection-borne terms and can be expressed as

$$\frac{\partial C(x,t)}{\partial t} = D \frac{\partial^2 C(x,t)}{\partial x^2} - V \frac{\partial C(x,t)}{\partial x} \quad 0 < x < L$$

where $C(x,t)$ is the concentration distribution of a macromolecule in the media as a function of radial distance x from the IEL and time t , and L is the thickness of the media. The boundary conditions are

$$D \frac{\partial C(x,t)}{\partial x} = P_{endo} \left[\frac{C(x,t)}{\varepsilon} - C_{endo}(t) \right] + VC(x,t) \quad x = 0$$

$$D \frac{\partial C(x,t)}{\partial x} = -P_{peri} \left[\frac{C(x,t)}{\varepsilon} - C_{peri}(t) \right] + VC(x,t) \quad x = L$$

and the initial condition is

$$C(x,t) = 0 \quad t \leq 0.$$

where $C_{endo}(t)$ and $C_{peri}(t)$ represent the endovascular and perivascular bulk phase concentrations as functions of time t , respectively. (The basic equation and boundary equations are derived from first principles in the Appendix.)

Other models have included effects not represented in this model such as reversible binding, dissociation, and intracellular degradation. These were not included in this analysis because fitting models with many parameters to a single concentration profile may lead to a mathematically underconstrained problem, i.e., a problem with too many degrees of freedom. This can lead to multiple solutions that fit the data with the same accuracy that depend on the initial parameter estimates used to start the fitting algorithm. It is then difficult to distinguish the "true" solution from other solutions. To reduce the possibility of these numerical complications, the model used incorporates only those mechanisms that appear to be dominant in the solute transport of dextrans. The effects not included in the model described may also be included in later analysis for a more complete model, one that contains more potential transport mechanisms.

IV.C. Perfusion Experiments

The transvascular transport of fluorescently labeled 20 kD dextrans in the calf carotid artery was examined using an *in vitro* perfusion apparatus that simulates plasma flow. Excess fascia and fat from calf carotid arteries was removed as previously described. A 15-25 mm artery segment without visible branches was then cannulated at both ends and tested for leaks by visually inspecting the vessel after connecting one end to an elevated lactated Ringer's solution source (Baxter) and closing off the other end. Intact arteries were placed in the perfusion apparatus for different durations. In addition

to separate endovascular and perivascular compartments which allow establishment of a transvascular concentration gradient, the apparatus can simulate plasma flow with varying pressure gradients. The perfusate flows from an upper reservoir through the artery, empties into a lower reservoir, and is pumped back to the upper reservoir with a hydrostatic pump. The height of the upper reservoir can be adjusted to establish a fixed transvascular pressure gradient and a separate reservoir for the perivascular bath allows establishment of transvascular concentration gradients. Perfusions were done at room temperature and the entire apparatus was enclosed in a wooden cabinet to prevent photobleaching of any fluorescent molecules.

This section describes a set of experiments to elucidate the vascular pharmacokinetics of 20 kD dextrans in the calf carotid artery. A similar experimental protocol utilizing this *in vitro* perfusion apparatus has been successful for investigating heparin transport in the rat abdominal aorta (Lovich and Edelman 1995). Dextrans should be placed either in the endovascular or perivascular bath, but not both, to separate the effects of transmural transport in each direction and simplify mathematical modeling. The last chapter showed that bath concentrations between 0.02 mg/ml to 2.5 mg/ml are necessary for the fluorescent signals be detectable. Therefore, 1 mg/ml can be used for the bath containing dextrans. Further investigation using 0.5 mg/ml may provide insight into mechanisms more dependent than convection and diffusion on absolute concentration such as binding and internalization. Convection is easily examined by applying no transvascular pressure gradient or a fixed value such as 100 cm to simulate a physiological pressure gradient. Multiple time points are necessary to estimate temporal aspects of a mathematical model. Einstein's solution to the one-dimensional Fick equation ($\bar{r}^2 = 2Dt$, where \bar{r}^2 is the mean-squared displacement a diffusing particle with effective diffusivity D travels after time t) suggest that experiments should be performed with durations that are separated by factors of 4 to allow temporal discrimination. Therefore, arteries could be perfused for 15 minutes, 1 hour, or 4 hours. Preliminary experiments shown in this chapter examined a small subset of the proposed experiments. Arteries were perfused for

one hour using an endovascular bath of 1 mg/ml of 20 kD FITC-Dx in PBS⁺⁺, and perivascular bath of PBS⁺⁺. There was no transvascular pressure gradient in these preliminary experiments, so any transport would be due solely to diffusion.

IV.D. Extraction of Concentration Profiles from Images

Perfused arteries were then processed using the procedure documented in the previous chapter. Transvascular concentration profiles were extracted with a user-assisted algorithm which prompts the user to delimit a 21 pixel thick region of media from the internal elastic lamina to the media-adventitia border. In anticipation of the extraction of the media, arterial cross-sections were oriented during imaging so that rectangular regions could be used to delimit the media. The 21 pixel thick region was averaged, giving a one-dimensional transvascular concentration profile. To reduce experimental variance, transvascular concentration profiles were constructed from five different cross-sections of the same artery and averaged with the average profile being truncated to the length of the shortest profile. Other studies have utilized a normalized distance from the endothelium with the distance of each point in the profile divided by the length of the media, resulting in distances ranging from 0 (the endothelium) to 1 (the media-adventitia border) (Bratzler, Chisolm et al. 1977; Ramirez, Colton et al. 1984; Penn, Koelle et al. 1990). This approximation may not be significant if the extracted media from cross-sections of the same artery have similar lengths. The procedure used in these studies did not use this approximation in an effort to maintain the spatial accuracy of individual profiles.

Two issues complicate the extraction of transvascular concentration profiles from two-dimensional images. The first is the inherent asymmetry of biological tissue which may cause substantial variability between profiles obtained from different transvascular regions of the same specimen. This complicates the process of averaging specimens to reduce experimental noise and suggests the need to image the identical transvascular region of different cross-sections when imaging. One possible solution would be to place fiduciary marks on the specimen block before sectioning. The other issue is the difficulty

discerning the edges of the media when extracting it from the artery. The media was extracted by a human operator using the UV image since the internal elastic lamina and adventitia tend to have greater fluorescence than the media in this image. After the user acquires some experience with extracting the media, this criteria is adequate for gross characterizations but may be inaccurate at the pixel level which has micron resolution with this technique. This is significant because fitting parameters such as the endovascular and perivascular permeabilities are heavily dependent on points near the boundaries of the delimited media.

IV.E. Determination of Transport Parameters

Transport parameters are determined by fitting a mathematical model of transport to measured concentration profiles. This procedure is not straightforward since the distributed model formulated earlier is described by partial differential equations and a function of continuous time and space, and each concentration profile is discrete in space and sampled at one instance in time. The method chosen in this study is to fit the concentration profile to simulations of the distributed model using finite difference approximations in space and Euler integration in time. A discrete concentration profile was simulated at evenly-spaced points throughout the media (x_1, \dots, x_N) . The endovascular and perivascular baths are assumed to be of constant concentration throughout the experiment:

$$\begin{aligned} C_{endo}(t) &= C_o \\ C_{peri}(t) &= C_1 \end{aligned}$$

and with no prior loading of the artery with dextrans, the initial conditions at each node are:

$$C(x_i, 0) = 0, \quad i = 1, \dots, N$$

Derivatives with respect to time in the governing transport equations were estimated by finite difference approximations:

$$\frac{\partial C(x_i, t)}{\partial x} \approx \frac{C(x_i, t) - C(x_{i-1}, t)}{\Delta x}$$

$$\frac{\partial^2 C(x_i, t)}{\partial x^2} \approx \frac{C(x_{i+1}, t) - 2C(x_i, t) + C(x_{i-1}, t))}{(\Delta x)^2}$$

where Δx represents the distance between two nodes x_i and x_{i+1} in the media. The distribution in the artery was then simulated by Euler integration in time:

$$C(x_i, t_{j+1}) \approx C(x_i, t_j) + \Delta t \frac{\partial C(x_i, t_j)}{\partial t}, \quad i = 1, \dots, N$$

$$\approx C(x_i, t_j) + \Delta t \left(D \frac{C(x_{i+1}, t_j) - 2C(x_i, t_j) + C(x_{i-1}, t_j))}{(\Delta x)^2} - V \frac{C(x_i, t_j) - C(x_{i-1}, t_j)}{\Delta x} \right),$$

$$i = 1, \dots, N$$

where Δt represents the increment (difference) between two time points t_j and t_{j+1} during Euler integration.

The transvascular transport model discussed in the previous section was implemented using MATLAB (MathWorks), a commercial programming language. The MATLAB program was then combined with a Nelder-Mead function-minimization routine to solve for transport parameters using an error criterion of the mean-square error between the experimental and simulated concentration profiles at each node. Model parameters are defined to be positive with no physical meaning otherwise. These positive restrictions were implemented by assigning a large error (10,000) to any profile obtained during parameter searches with negative parameters. Since the dimensions of each pixel are 1.326 μm by 1.326 μm and the thickness of the media of a calf carotid artery is approximately 400 μm , approximately 300 nodes would have to be used if every pixel is fit to a node. Preliminary studies showed that if the number of nodes was equal to the number of pixels needed to span the media, the computation time required for fitting would be prohibitive. Note that the parameter fitting routine must calculate the concentration at each node at every time increment during Euler integration. To reduce computation time, 40 nodes were defined across the media and the concentration at each

of these nodes was simulated. The corresponding concentration at each node of the experimental profile was then obtained by linear interpolation of the measured profile, and the mean-square error was computed using this interpolated profile and the simulated profile. One second was used as the time increment for Euler integration which was determined by using the largest increment possible without visible numerical instabilities.

With the assumptions and approximations described above, there are five transport parameters that need to be estimated in the parameter fitting routine: D , P_{endo} , P_{peri} , ε , and V . There are many practical issues involved with fitting experimental data to transport parameters in a mathematical model and this area needs further exploration. Preliminary experiments were done without transvascular pressure gradients, so the convective velocity (V) can be set to zero. The fraction of tissue space that 20 kD dextrans can distribute in the media was determined in the equilibrium studies described in the last chapter (Figure 7), so this parameter (ε) was fixed at 0.5233. This leaves three unknown parameters, the effective diffusivity and the endovascular and perivascular permeabilities, that need to be fitted.

Transport parameters were computed from transvascular concentration profiles of calf carotid arteries that were perfused for one and two hours at room temperature with no transvascular pressure gradient, and endovascular bath of 1 mg/ml FITC-Dx in PBS⁺⁺ and a perivascular bath of PBS⁺⁺ at room temperature. Figure 9 illustrates measured and simulated transvascular concentration profiles of arteries that were perfused for one hour, and Table 1 shows the initial and final parameter values and mean-square errors of the parameter fitting routine. Figure 10 illustrates measured and simulated transvascular concentration profiles of arteries that were perfused for two hours, and Table 2 shows the initial and final parameter values and mean-square errors of the parameter fitting routine.

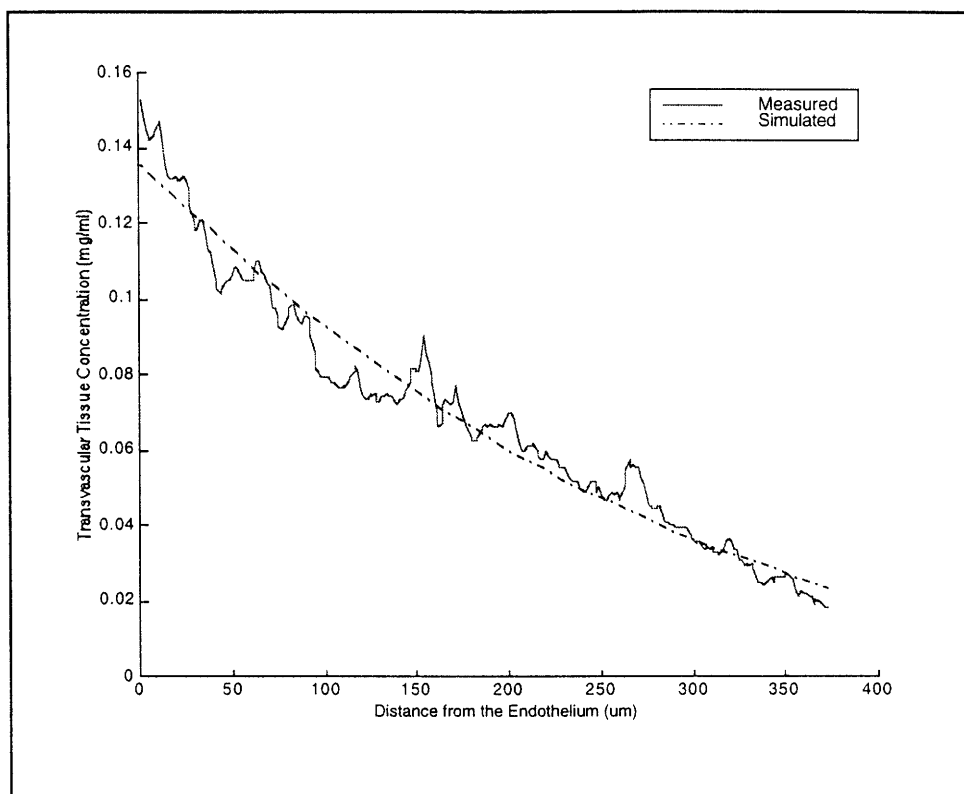


Figure 9. Concentration profiles for one hour perfusion data. Arteries were perfused for one hour with no transvascular concentration gradient, an endovascular bath of 1 mg/ml of FITC-Dx in PBS⁺⁺ and a perivascular bath of PBS⁺⁺. The measured concentration profile was then fit to a mathematical model of transvascular transport to yield a simulated profile.

Table 1. Parameter values and mean-square errors obtained when fitting one hour perfusion data

	Initial Values	Final Values
Diffusivity (D)	12 $\mu\text{m}^2/\text{s}$	15.29 $\mu\text{m}^2/\text{s}$
Endovascular Permeability (P_{endo})	110 $\mu\text{m}/\text{s}$	102.06 $\mu\text{m}/\text{s}$
Perivascular Permeability (P_{peri})	15 $\mu\text{m}/\text{s}$	18.88 $\mu\text{m}/\text{s}$
Mean-Square Error	7.68×10^{-5}	4.67×10^{-5}

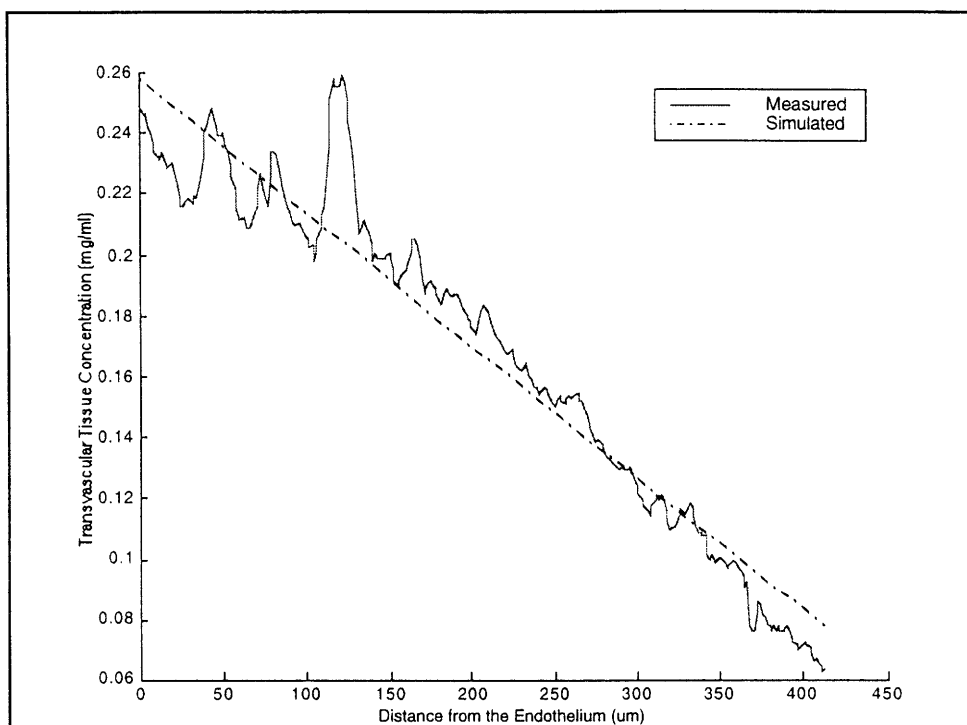


Figure 10. Concentration profiles for two hour perfusion data. Arteries were perfused for two hour with no transvascular concentration gradient, an endovascular bath of 1 mg/ml of FITC-Dx in PBS⁺⁺ and a perivascular bath of PBS⁺⁺. The measured concentration profile was then fit to a mathematical model of transvascular transport to yield a simulated profile.

Table 2. Parameter values and mean-square errors obtained when fitting two hour perfusion data

	Initial Values	Final Values
Diffusivity (D)	20 $\mu\text{m}^2/\text{s}$	44.22 $\mu\text{m}^2/\text{s}$
Endovascular Permeability (P_{endo})	50 $\mu\text{m}/\text{s}$	25.64 $\mu\text{m}/\text{s}$
Perivascular Permeability (P_{peri})	25 $\mu\text{m}/\text{s}$	7.83 $\mu\text{m}/\text{s}$
Mean-Square Error	2.55×10^{-4}	1.76×10^{-4}

The success of an optimization algorithm, such as the parameter fitting routine in these studies, is highly dependent on the estimated parameter values used to initiate the algorithm. Estimates of parameter values were not available since previous research on the transport of 20 kD dextrans in calf carotid arteries has been limited. An attempt to modify values from similar studies in our laboratories examining the transport of heparin, a similarly sized (6-30 kD) macromolecule, in the rat abdominal aorta were unsuccessful. Therefore, measured and simulated profiles were compared by a user and parameter values were adjusted until the profiles appeared similar. The fitting algorithm was then used to further optimize parameter values.

The discrepancy in parameter values obtained from the one and two hour perfusion data indicate that further investigation into both the experimental and mathematical methodology is necessary. However, it appears that it is feasible to calculate transport parameters by integrating the quantitative fluorescence microscopy technique developed in the last chapter with mathematical modeling.

IV.F. Chapter Summary

The method developed to quantify macromolecular distributions in vascular tissue described in the last chapter can be implemented with *in vitro* experiments to measure important transport mechanisms such as diffusion and convection. These measurements can then be used to construct better mathematical models which will further understanding of vascular transport and deposition. Experiments using fluorescently labeled 20 kD dextrans are proposed to demonstrate the measurement of transport parameters such as convective velocity, molecular diffusivity, and drug partitioning. The transport of macromolecules is dependent on factors such as the physico-chemical properties of the compound, state of the vessel and local environment. Similar experiments measuring these transport mechanisms would elucidate the relative importance of these factors. This could then be assimilated into general principles governing the transport and deposition of macromolecules in the vessel wall.

V. Conclusions

V.A. Accomplishments

Current methods to quantify macromolecular distributions in vascular tissues have been limited by post-experiment artifact, low signal-to-noise ratios, low spatial resolution, and the inability to provide multi-dimensional drug distribution profiles. This has suggested the need to develop new tools to obtain better experimental data. The quantitative fluorescent microscopy technique described in this work overcomes limitations of previous techniques and will be a valuable tool for investigation into the pharmacology and physiology of the vessel wall that determine the effect of bioactive molecules in tissues. This new technique can be incorporated into future experiments to gain insight into macromolecular transport and deposition within the vessel wall. This knowledge can then be applied to the rational design of drug delivery strategies. To illustrate the utility of this technique, the transvascular transport of fluorescently labeled 20 kD dextrans in the calf carotid artery was examined using an *in vitro* perfusion apparatus that simulates plasma flow. A mathematical model was fit to measured concentration profiles and provided estimates of important transport parameters such as the effective diffusivity within tissue, and endovascular and perivascular permeabilities.

V.B. Future Directions

The quantitative fluorescence microscopy technique developed in this thesis appears to be a very promising tool for future investigation into macromolecular pharmacokinetics in vascular tissue. The discrepancy between transport parameters obtained for the one hour and two hour perfusion data in the last chapter indicate that there are still issues to be resolved. Currently, we are attempting to compare this technique with *en face* serial sectioning to verify the accuracy of this technique. There are also numerical issues involved with fitting measured concentration profiles to a distributed model of transport that need to be investigated. The experimental data shown

here represent only a small portion of the different conditions that need to be examined to better understand macromolecular pharmacokinetics in the vessel wall. Future experiments and modeling need to examine issues such as the difference between endovascular and perivascular delivery, the effect of convective forces, and intermittent dosing.

In addition to examining different vessel conditions, this technique can be used to examine different compounds. One possible research direction is to isolate the effect that different physico-chemical properties have on the transport and deposition of a compound. One would expect that molecular size would be a major determinant, but the effects of other properties such as charge, solubility, and conformability, are often overlooked and may have substantial effect on the transport of a compound. As described in the previous chapter, dextrans are an ideal choice for these studies because their physico-chemical properties are easily modifiable. The results could then be used to develop a set of general principles that would predict the distribution of a compound based on its physico-chemical properties.

The ability to provide multi-dimensional concentration profiles was not exploited in this work, but may turn out to be one of this technique's most useful properties. It may not be desirable, or even possible, to completely expose a vessel that requires pharmacological treatment. Therefore, radially asymmetric delivery devices must be employed. There is a limited understanding of the distribution following administration from asymmetric devices, but the technique developed here may also be used to investigate this area.

VI. Appendix

VI.A. *Calculating Tissue Concentrations from Bulk Incubation Concentrations*

This section describes the derivation of an equation used to calculate the tissue concentration of a specimen which was incubated in a fixed bulk concentration and then reincubated in another bulk concentration to allow drug within the tissue to diffuse out of the tissue. Tissue concentrations are calculated for an original bulk incubation concentration of C_1 mg/ml, a bulk reincubation concentration of C_2 mg/ml, a wet tissue weight of x mg, and fractional volume ϵ . After the initial incubation, the amount of drug in the tissue (q mg) before reincubation is

$$q = \frac{\epsilon C_1 x}{\rho}$$

The drug redistributes in the reincubation bath (with volume V ml) and a mass balance yields

$$\begin{aligned} C_2 &= \frac{q}{V + \frac{\epsilon x}{\rho}} \\ &= \frac{\epsilon C_1 x}{V\rho + \epsilon x} \end{aligned}$$

Solving for the tissue concentration C_T yields

$$\begin{aligned} C_T &= \epsilon C_1 \\ &= \frac{C_2 (V\rho + \epsilon x)}{x} \end{aligned}$$

The volume of the reincubation bath is much larger than the fractional tissue volume available to the drug during the original incubation, allowing the following approximation to be made

$$V \gg \frac{\varepsilon x}{\rho} \Rightarrow V\rho \gg \varepsilon x$$

and the original tissue concentration to be approximated by

$$C_T \approx \frac{C_2 V \rho}{x}$$

VI.B. Derivation of Equations for a Mathematical Model of Transvascular Transport

The derivation of the basic equation of transvascular transport begins by defining $C(x, t)$ as the concentration of solute at a transvascular distance x from the internal elastic lamina and time t . Two mechanisms of solute transport are incorporated in this derivation: diffusion and convection. Diffusion across the element is proportional to the concentration gradient and convection across the element is proportional to the concentration at a particular point. In addition, both of these transport mechanisms are proportional to the cross-sectional area. The transvascular flux at distance x from the endothelium and time t , $j_{trans}(x, t)$, is the sum of these two components

$$\begin{aligned} j_{trans}(x, t) &= j_{diffusion}(x, t) + j_{convection}(x, t) \\ &= -AD \frac{\partial C(x, t)}{\partial x} + AVC(x, t) \end{aligned}$$

where the parameters D (length²/time) and V (length/time) represent the contributions due to diffusion and convection, respectively. Define a infinitesimal three-dimensional element centered at x , and let V_{elem} be the volume and A be the cross-sectional area of this infinitesimal element ($V_{elem} = A\Delta x$). A mass balance across this element (assuming there is no flux in the circumferential and longitudinal directions) yields the net flux across the infinitesimal element:

$$\begin{aligned}
j_{net}(x,t) &= j_{trans}(x,t) - j_{trans}(x + \Delta x, t) \\
&\approx j_{trans}(x,t) - \left(j_{trans}(x,t) + \frac{\partial j_{trans}(x,t)}{\partial x} \Delta x \right) \\
&= -\frac{\partial j_{trans}(x,t)}{\partial x} \Delta x \\
&= -\left(-AD \frac{\partial^2 C(x,t)}{\partial x^2} + AV \frac{\partial C(x,t)}{\partial x} \right) \Delta x \\
j_{net}(x,t) &= V_{elem} \left(D \frac{\partial^2 C(x,t)}{\partial x^2} - V \frac{\partial C(x,t)}{\partial x} \right)
\end{aligned}$$

The net flux (mass/time) divided by the element volume is identical to the change in concentration (mass/volume) with respect to time, therefore:

$$\begin{aligned}
\frac{\partial C(x,t)}{\partial t} &= \frac{j_{net}(x,t)}{V_{elem}} \\
&= D \frac{\partial^2 C(x,t)}{\partial x^2} - V \frac{\partial C(x,t)}{\partial x}
\end{aligned}$$

The derivation of the boundary equation for the luminal membrane corresponding to the endothelium and internal elastic lamina ($x = 0$) begins by defining an infinitesimal three-dimensional element centered at $x = 0$ with cross-sectional area A . In addition to the diffusive and convective effects described above for points within the media, there is an additional component due to permeation through the luminal membrane. The permeation across the luminal membrane is proportional to the concentration gradient across the membrane and the cross-sectional area of the element. This concentration gradient must be carefully defined since endovascular bath concentrations are expressed in bulk phase concentrations and concentrations in the media are expressed as tissue concentrations. The fraction of the tissue space the modeled compound can access must be used to express the concentration gradient properly. The net flux across this membrane is zero since the model assumes the membrane acts strictly as a barrier and does not store any drug. Therefore, the algebraic sum of the permeation, diffusion, and convection fluxes must equal zero:

$$j_{permeation}(0^-, t) + j_{diffusion}(0^+, t) + j_{convection}(0^+, t) = 0$$

$$P_{endo} A \left[\frac{C(0^+, t)}{\varepsilon} - C_{endo}(t) \right] + \left(-AD \frac{\partial C(0^+, t)}{\partial x} \right) + AVC(0^+, t) = 0$$

Rearranging terms gives the boundary equation for the endovascular membrane:

$$D \frac{\partial C(0^+, t)}{\partial x} = P_{endo} \left[\frac{C(0^+, t)}{\varepsilon} - C_{endo}(t) \right] + VC(0^+, t)$$

$$D \frac{\partial C(x, t)}{\partial x} = P_{endo} \left[\frac{C(x, t)}{\varepsilon} - C_o(t) \right] + VC(x, t), \quad x = 0$$

The derivation for the boundary equation for the perivascular membrane proceeds similarly.

VI.C. Programming Code for Transport Model and Parameter Fitting Routine

VI.C.1. Parameter Fitting Routine (ww_trans_fit.m)

```
% ww_trans_fit.m
%
% Parameter fitting algorithm. Calls "ww_trans_model" and "ww_trans_error"
%
% Wade Wan
% February 1, 1998

tic
% Load measured concentration profiles
pathstr='CORNHOLIO:Desktop Folder:CORNHOLIO Users:Wade:7/20/97 Analysis:';
cd(pathstr);
load bulk72097;

const=[];
for iii=1:3
switch iii
case 1,totalt=120;y=bulk72097(15:325,1);
case 2,totalt=90;y=bulk72097(5:315,2);
case 3,totalt=60;y=bulk72097(15:295,3);
end

x=(1:length(y))*1.326;
Eps=0.5233;
y=y*Eps;

% Fixed parameters
```



```

Cev=1;
Cpv=0;
V=0;
Lmed=length(y)*1.326;

% Variable parameters, [D Rend Radv]
paramorig=[20 50 25];

% disp. interm., tolerance for x, tolerance for F(x), .... max. eval.
% options(1),(2),(3),(14)_____default 0,1.e-4,1.e-4,....,200*length(x)
defaultopt=foptions;
% defaultopt(14)=5;
paramfit=fmins('ww_trans_error',paramorig,defaultopt,[],[totalt Cev Cpv V Lmed,Eps],y');

% ww_trans_model(D,Eps,Rend,Radv,totalt,Cev,Cpv,V,Lmed,testplot);
yfit=ww_trans_model(paramfit(1),Eps,paramfit(2),paramfit(3),totalt,Cev,Cpv,V,Lmed,0);
Nyfit=length(yfit)-2;
xfit=[0 (1:Nyfit)*Lmed/(Nyfit+1) Lmed];

hold on;
plot(x,y,'r',xfit,yfit,'b');
xlabel('Distance from the Endothelium (um)');
ylabel('Transvascular Tissue Concentration (mg/ml)');
title(['D Rend Radv=' num2str(paramorig) ' --> ' num2str(paramfit) '']);
hold off;
disp(paramfit);
const=[const; paramfit];
end % iii

toc

```

VI.C.2. Mathematical Model of Transport (ww_trans_model.m)

```

function [transprofile]=ww_trans_model(D,Eps,Rend,Radv,totalt,Cev,Cpv,V,Lmed,testplot);
% ww_trans_model.m
% function [transprofile]=ww_trans_model(D,Eps,Rend,Radv,totalt,Cev,Cpv,V,Lmed,testplot);
%
% Model of transvascular transport with nodes in the media, endovascular and perivascular permeabilities
%
% Wade Wan
% February 1, 1998

% Default Settings
if (nargin<1)
    D=12; % um^2/s
end
if (nargin<2)
    Eps=0.5; %
end
if (nargin<3)
    Rend=250; % s/um
end

```

```

end
if (nargin<4)
    Radv=60000;          % s/um
end
if (nargin<5)
    totalt=60;          % min
end
totalt=totalt*60; % min ---> s

if (nargin<6)
    Cev=1;              % mg/ml
end
if (nargin<7)
    Cpv=0;              % mg/ml
end
if (nargin<8)
    V=0;                %
end
if (nargin<9)
    Lmed=400;           % um
end
if (nargin<10)
    testplot=1;
end

dt=1;                  % s
ninc=totalt/dt;

Nmed=40;
Ntot=Nmed+2;           % One node at each boundary (endovascular, perivascular)
Lmednode=Lmed/(Nmed+1);

% Initial Loading Conditions
Cx_t = zeros(Ntot,ninc);
if (Rend==0)
    Cx_t(1,1)=Cev*Eps;
else
    Cx_t(1,1)=Cev*Lmednode*Eps/Rend/(D*Eps+Lmednode/Rend+V*Lmednode*Eps);
end

if (Radv==0)
    Cx_t(Ntot,1)=Cpv*Eps;
else
    Cx_t(Ntot,1)=Cpv*Lmednode*Eps/Radv/(D*Eps+Lmednode/Radv-V*Lmednode*Eps);
end

% Simulation
for xtime=2:ninc
    if (Rend==0)
        Cx_t(1,xtime)=Cev*Eps;
    else
        Cx_t(1,xtime)=(D*Eps*Cx_t(2,xtime-
1)+Cev*Lmednode*Eps/Rend)/(D*Eps+Lmednode/Rend+V*Lmednode*Eps);
    end
end

```

```

if (Radv==0)
    Cx_t(Ntot,xtime)=Cpv*Eps;
else
    Cx_t(Ntot,xtime)=(D*Eps*Cx_t(Ntot-1,xtime-1)+Cpv*Lmednode*Eps/Radv)/(D*Eps+Lmednode/Radv-
V*Lmednode*Eps);
end

d2C_dx2=(Cx_t(3:(Nmed+2),xtime-1)-2*Cx_t(2:(Nmed+1),xtime-1)+Cx_t(1:Nmed,xtime-
1))/(Lmednode^2);
dC_dx=(Cx_t(3:(Nmed+2),xtime-1)-Cx_t(2:(Nmed+1),xtime-1))/Lmednode;
dCx_t=D*d2C_dx2-V*dC_dx;
Cx_t(2:(Nmed+1),xtime)= Cx_t(2:(Nmed+1),xtime-1)+dCx_t*dt;
end % xtime
transprofile=Cx_t(:,ninc);

if (testplot==1)
% bndlength=50;
    hold on;
% plot(-bndlength:1:0,Cev*ones(bndlength+1,1),'g',...
%     Lmed:1:(Lmed+bndlength),Cpv*ones(bndlength+1,1),'g',...
%     [0 0],[0 max([Cpv Cev])], 'm', ...
%     [Lmed Lmed],[0 max([Cpv Cev])], 'm');

% xlabel('Distance from Endothelium/IEL (um)');
% ylabel('Concentration (mg/ml)');
xvar=[0 (1:Nmed)*Lmednode Lmed];
plot(xvar,transprofile,'-.');
% yheight=1.25*max(Cx_t(:,ninc));
% axis([-bndlength Lmed+bndlength 0 yheight]);
% title(['[D Eps Rend Radv t V] =' num2str([D Eps Rend Radv totalt/60 V])]);
% text(-bndlength*3/4,yheight*0.9,'EV');
% text(Lmed/4,yheight*0.9,'Media');
% text(Lmed+bndlength/4,yheight*0.9,'PV');
    hold off;
end

```

VI.C.3. Error Function (ww_trans_error.m)

```

function ferror=ww_trans_error(param_alter,param_fix,data)
% ww_trans_error.m
% function ferror=ww_trans_error(param_alter,param_fix,data)
%
% Calculates the error between measured and simulated profiles for use with "fmins"
%
% Wade Wan
% February 1, 1998

% Variable parameters
D=param_alter(1);
Rend=param_alter(2);

```

```

Radv=param_alter(3);

% Fixed parameters
totalt=param_fix(1);
Cev=param_fix(2);
Cpv=param_fix(3);
V=param_fix(4);
Lmed=param_fix(5);
Eps=param_fix(6);

if min(param_alter)<0
    ferror=10000;
    disp(['***Negative Parameter: ' num2str(ferror) ' =====> Parameters: ' num2str(param_alter)]);
else
    %simy=ww_trans_model(D,Eps,Rend,Radv,totalt,Cev,Cpv,V,Lmed,0);
    simy=ww_trans_model(D,Eps,Rend,Radv,totalt,Cev,Cpv,V,Lmed,0);
    Nsim=length(simy)-2;
    simx=[0 (1:Nsim)*Lmed/(Nsim+1) Lmed];

    Nexp=length(data)-2;
    expx=[0 (1:Nexp)*Lmed/(Nexp+1) Lmed];
    expy=interp1(expx,data,simx,'*linear');
    % Interpolates to find corresponding concentrations in measured profile

    plot(simx,simy,'x',simx,expy,'o');
    legend('Simulation','Experimental');
    ferror=mean((simy-expy).^2);
    disp(['Error: ' num2str(ferror) ' =====> Parameters: ' num2str(param_alter)]);
    drawnow;
end

```

VI.D. Experimental Data

Table 3. Experimental data for Figure 3 (Tissue Concentration as a Function of Incubation Time)

Incubation Time (hr)	Tissue Concentration (mg/ml)			Mean	Standard Deviation
	# 1	# 2	# 3		
1	0.48	0.43	0.48	0.46	0.03
2	0.42	0.44	0.49	0.45	0.04
4	0.46	0.59	0.57	0.54	0.07
6	0.56	0.57	0.62	0.58	0.03
16	0.61	0.56	0.55	0.57	0.03
20	0.59	0.62	0.60	0.60	0.02
24	0.60	0.61	0.59	0.60	0.01
40	0.57	0.65	0.59	0.60	0.04
48	0.55	0.61	0.63	0.60	0.04

Table 4. Experimental data for Figure 6 (Fluorescent Intensity as a Function of Incubation Concentration)

Incubation Concentration (mg/ml)	Specimen #	Section #	Mean	Standard Deviation
2.50	2	4	145.88	10.25
2.50	2	5	163.64	11.56
2.50	2	6	166.13	8.05
			158.55	5.81
2.00	2	4	145.94	13.70
2.00	2	5	152.10	18.06
2.00	2	6	126.21	10.01
			141.41	8.26
1.00	2	4	100.41	8.47
1.00	2	5	76.82	6.81
1.00	2	6	80.96	10.00
			86.06	4.92
0.50	1	4	58.25	4.53
0.50	1	5	49.85	4.02
0.50	1	6	55.75	4.33
			54.62	2.48
0.25	2	4	43.38	3.92
0.25	2	5	34.76	5.87
0.25	2	6	50.77	3.17
			42.97	2.58
0.20	1	4	38.44	3.03
0.20	1	5	31.13	2.79
0.20	1	6	40.99	2.67
			36.85	1.64
0.15	1	4	23.99	2.21
0.15	1	5	36.05	2.49
0.15	1	6	37.84	3.29
			32.63	1.56
0.10	2	4	15.31	1.76
0.10	2	5	16.46	1.98
0.10	2	6	23.16	4.00
			18.31	1.60
0.05	2	4	6.77	1.77
0.05	2	5	6.81	2.85
0.05	2	6	8.18	2.05
			7.25	1.31
0.02	2	4	3.59	1.42
0.02	2	5	4.66	1.52
0.02	2	6	5.66	1.41
			4.64	0.84

Table 5. Experimental data for Figure 7 (Tissue Concentration as a Function of Bulk Phase Concentration)

Bulk Phase Concentration (mg/ml)	Tissue Concentration (mg/ml)			Mean	Standard Deviation
	# 1	# 2	# 3		
0.5	0.334	0.284	0.315	0.311	0.025
0.6	0.325	0.353	0.281	0.320	0.036
0.7	0.374	0.419	0.375	0.389	0.026
0.8	0.386	0.342	0.476	0.401	0.068
0.9	0.455	0.399	0.462	0.439	0.034
1.0	0.497	0.534	0.534	0.522	0.021

References

Aitken, W. M., E. Wright, et al. (1968). "Autoradiography of Water-Diffusible Substances in Sections of Whole Baby Rats." Stain Technology **43**: 1-7.

Armenante, P. M., D. Kim, et al. (1991). "Experimental Determination of the Linear Correlation between in Vivo TV Fluorescence Intensity and Vascular and Tissue FITC-DX Concentrations." Microvascular Research **42**: 198-208.

Bell, F. P., I. L. Adamson, et al. (1974). "Aortic Endothelial Permeability to Albumin: Focal and Regional Patterns of Uptake and Transmural Distribution of ^{131}I -Albumin in the Young Pig." Experimental and Molecular Pathology **20**: 57-68.

Bell, F. P., A. S. Gallus, et al. (1974). "Focal and Regional Patterns of Uptake and the Transmural Distribution of ^{131}I -Fibrinogen in the Pig Aorta *in Vivo*." Experimental and Molecular Pathology **20**: 281-292.

Bratzler, R. L., G. M. Chisolm, et al. (1977). "The Distribution of Labeled Low-Density Lipoproteins Across the Rabbit Thoracic Aorta in Vivo." Atherosclerosis **28**: 289-307.

Bratzler, R. L., G. M. Chisolm, et al. (1977). "The Distribution of Labeled Albumin across the Rabbit Thoracic Aorta in Vivo." Circulation Research **40**: 182-190.

Castellot, J. J., K. Wong, et al. (1985). "Binding and Internalization of Heparin by Vascular Smooth Muscle Cells." Journal of Cellular Physiology **124**: 13-20.

Chuang, P., H. Cheng, et al. (1990). "Macromolecular Transport across Arterial and Venous Endothelium in Rats." Arteriosclerosis **10**: 188-197.

Cowen, T., A. J. Haven, et al. (1985). "Pontamine sky blue: A counterstain for background autofluorescence in fluorescence and immunofluorescence histochemistry." Histochemistry **82**: 205-208.

Duncan, L. E., K. Buck, et al. (1963). "Lipoprotein Movement through Canine Aortic Wall." Science **142**: 972-973.

Duncan, L. E., J. Cornfield, et al. (1959). "Circulation of Labeled Albumin Through the Aortic Wall of the Dog." Circulation Research **7**: 390-397.

Fox, J. R. and H. Wayland (1979). "Interstitial Diffusion of Macromolecules in the Rat Mesentery." Microvascular Research **18**: 255-276.

Fry, D. L. (1985). "Mathematical models of arterial transmural transport." Am. J. Physiol. **248**: H240-H263.

Fry, D. L., R. W. Mahley, et al. (1980). "Quantitative microautoradiography of arteries: comparison of radioactivity to silver." Am. J. Physiol. **239**: H289-H295.

Halldén, G., C. M. Sköld, et al. (1991). "Quenching of intracellular autofluorescence in alveolar macrophages permits analysis of fluorochrome labelled surface antigens by flow cytofluorometry." Journal of Immunological Methods **142**: 207-214.

Kao, C. H., J. K. Chen, et al. (1995). "Visualization of the transport pathways of low density lipoproteins across the endothelial cells in the branched regions of rat arteries." Atherosclerosis **116**: 27-41.

Kong, J. and D. P. Ringer (1995). "Quantitative *in Situ* Image Analysis of Apoptosis in Well and Poorly Differentiated Tumors from Rat Liver." American Journal of Pathology **147**(1626-1632).

Koppel, D. E., C. Carlson, et al. (1989). "Analysis of heterogeneous fluorescence photobleaching by video kinetics imaging: the method of cumulants." Journal of Microscopy **155**: 199-206.

Langer, R. and M. Moses (1991). "Biocompatible Controlled Release Polymers for Delivery of Polypeptides and Growth Factors." Journal of Cellular Biochemistry **45**: 340-345.

Lovich, M. A. and E. R. Edelman (1995). "Mechanisms of Transmural Heparin Transport in the Rat Abdominal Aorta After Local Vascular Delivery." Circulation Research **77**: 1143-1150.

Lovich, M. A. and E. R. Edelman (1996). "Computational simulations of local vascular heparin deposition and distribution." Am. J. Physiol. **271**: H2014-H2024.

Marriott, G., R. M. Clegg, et al. (1991). "Time resolved imaging microscopy: Phosphorescence and delayed fluorescence imaging." Biophysical Journal **60**: 1374-1387.

Nakamura, Y. and H. Wayland (1975). "Macromolecular Transport in the Cat Mesentery." Microvascular Research **9**: 1-21.

Nimni, M. E. (1997). "Polypeptide growth factors: targeted delivery systems." Biomaterials **18**: 1201-1225.

Nugent, L. J. and R. K. Jain (1984). "Plasma pharmacokinetics and interstitial diffusion of macromolecules in a capillary bed." Am. J. Physiol. **246**: H129-H137.

Penn, M. S. and G. M. Chisolm (1991). "Relation Between Lipopolysaccharide-Induced Endothelial Cell Injury and Entry of Macromolecules Into the Rat Aorta In Vivo." Circulation Research **68**: 1259-1269.

Penn, M. S., M. R. Koelle, et al. (1990). "Visualization and Quantification of Transmural Concentration Profiles of Macromolecules Across the Arterial Wall." Circulation Research **67**: 11-22.

Penn, M. S., G. M. Saidel, et al. (1992). "Vascular injury by endotoxin: changes in macromolecular transport parameters in rat aortas in vivo." Am. J. Physiol. **262**: H1563-H1571.

Penn, M. S., G. M. Saidel, et al. (1994). "Relative Significance of Endothelium and Internal Elastic Lamina in Regulating the Entry of Macromolecules Into Arteries In Vivo." Circulation Research **74**: 74-82.

Ramirez, C., C. Colton, et al. (1984). "Transport of ^{125}I -Albumin Across Normal and Deendothelialized Rabbit Thoracic Aorta In Vivo." Arteriosclerosis **4**: 283-291.

Rogers, C. and E. R. Edelman (1995). "Endovascular Stent Design Dictates Experimental Restenosis and Thrombosis." Circulation **91**: 2995-3001.

Ross, R. (1993). "The pathogenesis of atherosclerosis: a perspective for the 1990s." Nature **362**: 801-809.

Rutledge, J. C., F. E. Curry, et al. (1990). "Low Density Lipoprotein Transport Across a Microvascular Endothelial Barrier After Permeability Is Increased." Circulation Research **66**: 486-495.

Saidel, G. M., E. D. Morris, et al. (1987). "Transport of Macromolecules in Arterial Wall *In Vivo*: A Mathematical Model and Analytical Solutions." Bulletin of Mathematical Biology **49**: 153-169.

Schnitzer, J. J., E. M. Morrel, et al. (1987). "Absolute Quantitative Autoradiography of Low Concentrations of [^{125}I]-Labeled Proteins in Arterial Tissue." The Journal of Histochemistry and Cytochemistry **35**: 1439-1450.

Schwartz, R. S., K. C. Huber, et al. (1992). "Restenosis and the Proportional Neointimal Response to Coronary Artery Injury: Results in a Porcine Model." J. Am. Coll. Cardiol. **19**: 267-274.

Seveus, L., M. Väisälä, et al. (1992). "Time-Resolved Fluorescence Imaging of Europium Chelate Label in Immunohistochemistry and In Situ Hybridization." Cytometry **13**: 329-338.

Steinkamp, J. A. and C. C. Stewart (1986). "Dual-Laser, Differential Fluorescence Correction Method for Reducing Cellular Background Autofluorescence." Cytometry **7**: 566-574.

Szöllösi, J., S. J. Lockett, et al. (1995). "Autofluorescence Correction for Fluorescence In Situ Hybridization." Cytometry **20**: 356-361.

Tedgui, A., R. Merval, et al. (1992). "Albumin Transport Characteristics of Rat Aorta in Early Phase of Hypertension." Circulation Reserach **71**: 932-942.

Tompkins, R. G., M. L. Yarmush, et al. (1989). "Low-density lipoprotein transport in bloodvessel walls of squirrel monkeys." Am. J. Physiol. **257**: H452-H464.

van de Lest, C. H. A., E. M. M. Versteg, et al. (1995). "Elimination of Autofluorescence in Immunofluorescence Microscopy with Digital Image Processing." The Journal of Histochemistry and Cytochemistry **43**: 727-730.

Weinberg, P. D. (1988). "Application of fluorescence densitometry to the study of net albumin uptake by the rabbit aortic wall up- and downstream of intercostal ostia." Atherosclerosis **74**: 139-148.